

This document was prepared in conjunction with work accomplished under Contract No. DE-AC09-96SR18500 with the U. S. Department of Energy.

DISCLAIMER

This report was prepared as an account of work sponsored by an agency of the United States Government. Neither the United States Government nor any agency thereof, nor any of their employees, nor any of their contractors, subcontractors or their employees, makes any warranty, express or implied, or assumes any legal liability or responsibility for the accuracy, completeness, or any third party's use or the results of such use of any information, apparatus, product, or process disclosed, or represents that its use would not infringe privately owned rights. Reference herein to any specific commercial product, process, or service by trade name, trademark, manufacturer, or otherwise, does not necessarily constitute or imply its endorsement, recommendation, or favoring by the United States Government or any agency thereof or its contractors or subcontractors. The views and opinions of authors expressed herein do not necessarily state or reflect those of the United States Government or any agency thereof.

EVALUATION OF TECHNOLOGIES TO COMPLEMENT/REPLACE MASS SPECTROMETERS IN THE TRITIUM FACILITIES (U)

L. L. Tovo, R. J. Lascola, W. A. Spencer, C. S. McWhorter, K. E. Zeigler

August 30, 2005

UNCLASSIFIED

DOES NOT CONTAIN
UNCLASSIFIED CONTROLLED
NUCLEAR INFORMATION

ADC&

Reviewing

Official: Laura L. Tovo, Fellow Scientist.
(Name and Title)

Date: September 1, 2005

Westinghouse Savannah River Company
Savannah River National Laboratory
Aiken, SC 29808

Prepared for the U.S. Department of Energy Under
Contract Number DEAC09 -96SR18500



SRNL
SAVANNAH RIVER NATIONAL LABORATORY

DISCLAIMER

This report was prepared by Westinghouse Savannah River Company (WSRC) for the United States Department of Energy under Contract No. DE-AC09-96SR18500 and is an account of work performed under that contract. Neither the United States Department of Energy, nor WSRC, nor any of their employees makes any warranty, expressed or implied, or assumes any legal liability or responsibility for the accuracy, completeness, or usefulness, of any information, apparatus, or product or process disclosed herein or represents that its use will not infringe privately owned rights. Reference herein to any specific commercial product, process, or service by trademark, name, manufacturer or otherwise does not necessarily constitute or imply endorsement, recommendation, or favoring of same by WSRC or by the United States Government or any agency thereof. The views and opinions of the authors expressed herein do not necessarily state or reflect those of the United States Government or any agency thereof.

Printed in the United States of America

**Prepared For
U.S. Department of Energy**

Key Words:

*Mass Spectrometer,
Raman, Sensors, Gas Analysis*

Retention: Permanent

**EVALUATION OF TECHNOLOGIES TO
COMPLEMENT/REPLACE MASS SPECTROMETERS IN
THE TRITIUM FACILITIES (U)**

L. L. Tovo, R. J. Lascola, W. A. Spencer, C. S. McWhorter, K. E. Zeigler

August 30, 2005

UNCLASSIFIED

DOES NOT CONTAIN
UNCLASSIFIED CONTROLLED
NUCLEAR INFORMATION

ADC&

Reviewing

Official: Laura L. Tovo, Fellow Scientist
(Name)

Date: September 1, 2005

Westinghouse Savannah River Company
Savannah River National Laboratory
Aiken, SC 29808

Prepared for the U.S. Department of Energy Under
Contract Number DEAC09 -96SR18500



SRNL
SAVANNAH RIVER NATIONAL LABORATORY

REVIEWS AND APPROVALS

AUTHOR(S):

Laura L. Tovo 8/31/05
 L. L. Tovo, Analytical Development Section Date

Robert J. Lascola 9/6/05
 R. J. Lascola, Analytical Development Section Date

W.A. Spencer 8/31/2005
 W. A. Spencer, Analytical Development Section Date

C. S. McWhorter 8/31/2005
 C. S. McWhorter, Analytical Development Section Date

K. E. Zeigler 8/31/2005
 K. E. Zeigler, Analytical Development Section Date

TECHNICAL REVIEWER:

W. T. Boyce 9-1-05
 W. T. Boyce, Analytical Development Section Date

APPROVERS

L. M. Chandler 9-1-05
 L. M. Chandler, Manager, Analytical Development Section Date

S. Wyrick 9/6/05
 S. Wyrick, Manager, Hydrogen Technology Section Date

EXECUTIVE SUMMARY

The problem of the aging mass spectrometers coupled with lack of vendor support and no viable commercially available replacement presents risks for process control and monitoring in the Tritium Facilities. Therefore, several technologies were evaluated to maintain and, if possible, to enhance the current analytical capabilities provided by the existing mass spectrometers. These technologies included potential replacement/complement mass spectrometers as well as on-line sensors. Based on the results of this evaluation, the Savannah River National Laboratory (SRNL) makes the following recommendations.

- Work should begin on implementation of the Quantra Fourier Transform-Ion Cyclotron Resonance (FT-ICR) as a complement to the existing mass spectrometers or as an on-line process analyzer. In its current configuration, the instrument can measure masses 12 or greater, with a resolution of 30,000 at mass 28, and 100 part per million detection limit using ion ejection of major ions. Thus, the 16-24 mass region that is not so easily separated by the existing Tritium Facility mass spectrometers could be resolved and measured using the FT-ICR. For the FT-ICR (Quantra) to be of even more benefit to the Tritium Facilities, it should be re-engineered to provide analysis of masses 2-1000 in a single scan as well as other hardware and software improvements identified during our evaluation (i.e. long term stability, quantitative analysis of mixtures, etc.). In collaboration, SRS, LANL, and Y12 have secured funding for this project and the re-engineering effort will begin in FY06. Once the re-engineering effort is complete, funding will be required for performance testing and implementation in a tritiated environment as well as validation with the design agency.
- The bench top magnetic sector mass spectrometer (GCMATE) technology closely matches that of the existing mass spectrometers in the Tritium Facilities. The initial work with the GCMATE indicates that its resolution and sensitivity meet the requirements of a replacement mass spectrometer for the Tritium Facilities. Although this instrument appears to be the most promising as a replacement for the existing mass spectrometers, delayed funding in FY05 precluded a complete evaluation. Therefore, evaluation of this instrument should continue in FY06.
- Fiber optic Raman Spectroscopy has been demonstrated as a useful on-line technology for measurement of hydrogen isotopes at a concentration of greater than 1%. The method should be demonstrated on a process containing tritium. Upon successful demonstration in a tritium process, the method should then be implemented on the Hydrogen-Tritium Thermal Cycling Adsorption Process (HT-TCAP) and other processes that would require a detection limit of 1% or greater. Research and development to improve the detection limit of the fiber optic Raman method should continue as this would allow on-line analysis of other process points (i.e. HT-TCAP product and raffinate, Tritium Process Stripper, etc.).
- The on-line vapochromic sensor for ammonia should be implemented in processes that require detection of an ammonia concentration greater than 0.5%. However, most processes in the Tritium Facilities require detection of low ppm concentration and therefore, the on-line vapochromic sensor work will not be pursued further.
- Infrared plug sensors can be expected to provide measurements of gas concentrations within 2-3% at atmospheric pressures. They are not suitable for trace gas detection without substantial

modification. Research and development for sensors (i.e. photoacoustic, infrared) that can detect trace (less than 100 ppm) amounts of ammonia, water and hydrocarbons (i.e. methane) should continue.

TABLE OF CONTENTS

| | |
|--|-----|
| EXECUTIVE SUMMARY | iii |
| LIST OF FIGURES | vii |
| LIST OF TABLES | ix |
| LIST OF ACRONYMS | x |
| 1.0 INTRODUCTION AND BACKGROUND | 1 |
| 2.0 Mass Spectrometer | 3 |
| 2.1 Introduction | 3 |
| 2.2 Experimental | 6 |
| 2.2.1 Siemens Quantra FT-ICR | 6 |
| 2.2.2 JEOL GCMATE II Bench Top Magnetic Sector Mass Spectrometer | 9 |
| 2.3 Results and Discussion | 12 |
| 2.3.1 Evaluation of the Siemens Quantra FT-ICR | 12 |
| 2.3.2 Ion Trap Optimization and ionization current | 15 |
| 2.3.3 Helium and Deuterium on the Quantra | 16 |
| 2.3.4 Evaluation of the JEOL GCMATE II BenchTop Magnetic Sector Mass Spectrometer | 18 |
| 2.4 Conclusions and Recommendations | 19 |
| 3.0 Fiber Optic Raman Spectroscopy | 21 |
| 3.1 Introduction | 21 |
| 3.2 Experimental | 23 |
| 3.3 Results and Discussion | 25 |
| 3.3.1 Proof of Concept | 25 |
| 3.3.2 HT-TCAP DEMO | 25 |
| 3.3.2.1 Advantages over RGA | 32 |
| 3.3.2.2 Exchange Tests | 33 |
| 3.3.2.3 Path forward | 33 |
| 3.4 Conclusions and Recommendations | 33 |
| 4.0 Vapochromic Sensors | 35 |
| 4.1 Introduction and Background | 35 |
| 4.2 Experimental | 36 |
| 4.2.1 Gas Generation System | 36 |
| 4.2.2 Vapochromic Sensor Probe | 36 |
| 4.2.3 Partial least squares analysis | 36 |
| 4.3 Results | 37 |
| 4.4 Conclusions | 42 |
| 4.5 Recommendations/Path Forward | 42 |
| 5.0 Miniature Infrared Sensors | 43 |
| 5.1 Introduction and Background | 43 |
| 5.2 Experimental | 44 |
| 5.2.1 Sensors | 44 |
| 5.2.2 Gas Handling | 46 |
| 5.2.3 Calculations | 46 |
| 5.3 Results and Discussion | 47 |

| | |
|--|----|
| 5.3.1 Experimental Results | 47 |
| 5.3.2 Sensor Stability | 47 |
| 5.3.3 CO Sensor | 49 |
| 5.3.4 H ₂ O Sensor | 50 |
| 5.3.5 Analyte Independence | 50 |
| 5.3.6 Signal Averaging | 52 |
| 5.4 Calculation Results | 53 |
| 5.4.1 Methodology | 54 |
| 5.4.2 Comparison to Experiment | 54 |
| 5.4.3 Temperature Effects on Water Absorbances | 56 |
| 5.4.4 Pressure Broadening | 56 |
| 5.5 Conclusions and Recommendations | 57 |
| 6.0 REFERENCES | 59 |

LIST OF FIGURES

| | | |
|-----------|--|----|
| Figure 1 | A) Siemens Applied Automation Quantra portable FT-ICR mass spectrometer with inlet system designed at SRNL. Dimensions are 42 inches high, 22 inches wide, and 24 inches deep. B) View inside the cabinet of the Quantra system. The FT-ICR cell is inside the round cylinder in the cabinet. | 7 |
| Figure 2 | Sample inlet system for the Siemens Quantra using Swagelok IGC II manifolds and pneumatic controlled valves. The piezo-electric valves were heated and visible as the red lines in the photograph. | 8 |
| Figure 3 | Sample inlet computer control and trending of the sample inlet pressure. Piezo1 and Piezo2 are the Quantra inlet valves. | 9 |
| Figure 4 | JEOL GCMATE II Gas Chromatography Mass Spectrometer System. The gas chromatograph has been removed from the inlet to the mass spectrometer for the evaluation studies. | 10 |
| Figure 5 | JEOL GCMATE Ion Source | 11 |
| Figure 6 | The initial test inlet system used a 1 liter sample expansion volume to lower inlet pressures and improve flow across the variable leak. | 12 |
| Figure 7 | Carbon dioxide, nitrous oxide (N ₂ O), and propane(C ₃ H ₈) could be separately analyzed. Mass calibration in this image is biased 0.02 amu low. | 13 |
| Figure 8 | Background oil at low 8 K resolution. Major ions have been ejected. | 14 |
| Figure 9 | Background oils at high 131K resolution. Major ions have been ejected. | 14 |
| Figure 10 | Sniffing ammonia and methane in air. Siemens software tracks ions in time but very close masses were difficult to setup to track independently. This examples shows ¹⁶ O and CH ₄ were tracked but OH and ammonia were not. The isense value is a measure of the total internal ion current of the system. | 15 |
| Figure 11 | Filament Current Optimization. | 16 |
| Figure 12 | Inlet Pressure vs Detection Saturation for Helium and Deuterium | 17 |
| Figure 13 | Detector and Isense Ranges. | 18 |
| Figure 14 | Helium and Deuterium separation using the GCMATE II. The resolution is 4100. | 19 |
| Figure 15 | Schematic of fiber-optic laser Raman set-up; | 23 |
| Figure 16 | Raman System Components: | 24 |
| Figure 17 | Typical Raman spectra from HT-TCAP cold runs. A. represents a 50:50 mixture at the midpoint. The baseline is choppy because of a light leak from the RGA sampling point across from the Raman probe head in the process tee. B. Represents a 5:95 mixture closer to the raffinate end. D ₂ cannot be seen because the concentration is at the detection limit for the analysis. | 26 |
| Figure 18 | Real time measurement using Raman. This example of the 40:60 D ₂ :H ₂ mixture shows that Raman can be used to watch the isotope sweep across the midpoint. As seen here, when the heating cycle begins, D ₂ is most abundant at the midpoint. Because the column has an affinity for the H ₂ , it is slower to leave the column. As the heating cycle continues the H ₂ is released. Over time, the H ₂ continues to move down the column and that is the most abundant isotope seen at the midpoint. | 31 |
| Figure 19 | Cold Run testing for 40:60 D ₂ :H ₂ . Plot of % ratio of the isotopes versus time. At time 0, the hot cycle begins, and at time 15, the hot cycle ends and the cooling of the column begins. | |

The relative percents at the ending point are 67% H₂ and 33% D₂. (HD was not calculated into these percentages but would be about the correct ratio if added to each of the H₂ and D₂.)

| | |
|---|----|
| | 32 |
| Figure 20 Emission profile of vapochrome compound in the presence of 0 and 100% relative humidity | 35 |
| Figure 21 Picture of the sensor probe inside incubator chamber. SSFM - stainless steel flow mount, RP - reflectance probe, PT - pressure transduce, RTD - temperature transducer..... | 36 |
| Figure 22 Luminescence spectra of [Pt(phen)(CN-cyclododecyl) ₄][Pt(CN) ₄] after exposure to increasing ammonia concentration. | 38 |
| Figure 23 PLS calibration model over 0.3 to 3.0% ammonia. The model captures 97% of the variance in the data. | 39 |
| Figure 24 PLS calibration model over 0.7 to 3.0% ammonia. The model captures over 99% of the variance in the data. | 40 |
| Figure 25 PLS loadings plot over the 0.3 to 3.0% ammonia calibration range. PC1 describes the variance associated with the increase in intensity, PC2 describes the variance due to the bathochromic shift with change concentration and PC3 describes the variance due to residual wavelength shifting at the lower concentration ranges. | 41 |
| Figure 26 Photograph of infrared cell..... | 45 |
| Figure 27 Spectral profiles of IR filters and source..... | 45 |
| Figure 28 Stability and noise characteristics of detectors..... | 48 |
| Figure 29 Relationship between pressure and absorbance for CO..... | 49 |
| Figure 30 Relationship between pressure and absorbance for H ₂ O. | 51 |
| Figure 31 Pressure-dependent deviation from ideal gas law..... | 52 |
| Figure 32 Effect of signal averaging..... | 53 |
| Figure 33 Relationship of pathlength and absorbance..... | 55 |

LIST OF TABLES

| | |
|---|----|
| Table 1 Hydrogen and helium isotopic masses..... | 3 |
| Table 2 Resolution of Ion Pairs..... | 4 |
| Table 3 Common ions in light gas mixtures..... | 5 |
| Table 4 50:50 D ₂ :H ₂ mixture results for the midpoint of column C. Results compare to those obtained by the on-line Raman analysis and the samples that were pulled for laboratory mass spectrometer measurements. Results agree to within 6% and discounting the HD, agree to within 3%..... | 27 |
| Table 5 Comparison of off-line analysis versus the Raman results for 5:95 D ₂ :H ₂ mixtures. This data was taken from an area positioned closer to the raffinate end. The top chart represents the hot cycle (pressure of about 2000 torr) and the comparison between the lab mass spectrometer and Raman results. Again, D ₂ was at its detection limit with the Raman therefore, it could not be seen. The bottom chart represents the beginning of the cold cycle (about 1400 torr of pressure) and the comparison of the RGA results and Raman results. Again, the limit of detection for D ₂ is about 1% and the amount of D ₂ at this position is much less than that. The HD measurements in both cases were reaching the detection limits as well, so the percent differences are much greater. | 28 |
| Table 6 More comparison results for 5:95 D ₂ :H ₂ mixtures. The probe was positioned closer to the raffinate end. The HD was reaching its detection limit while the D ₂ was at its detection limit. Results are in good agreement between the RGA, lab mass spectrometer and Raman..... | 29 |
| Table 7 Qualitative luminescence properties of screened vapochromic compounds. Ratings: 1 = good, 2 = useable, 3 = minimal response and 4 = no response. | 37 |
| Table 8 Temperature dependence of CO absorbance..... | 50 |
| Table 9 Temperature dependence of CO and H ₂ O absorbance..... | 56 |
| Table 10 Pressure broadening of CO, H ₂ O absorbance..... | 57 |

LIST OF ACRONYMS

| | |
|----------------------|--|
| ADAPT | Advanced Design and Production Technologies |
| ADS | Analytical Development Section |
| amu | atomic mass unit |
| au | Absorbance units |
| CCD | charge-coupled device |
| D₂ | deuterium |
| DOE | Department of Energy |
| FFT | Fast Fourier Transform |
| FT-ICR | Fourier Transform Ion Cyclotron Resonance |
| GC | Gas chromatography |
| H₂ | protium |
| HD | protium-deuterium |
| HT-TCAP | hydrogen-tritium thermal cycling absorption process |
| IR | Infrared (absorption spectroscopy) |
| KV | kilovolts |
| LANL | Los Alamos National Laboratory |
| MHz | megahertz |
| MS | mass spectrometry |
| mW | milliWatts |
| m/z | mass to charge ratio |
| nm | nanometer |
| PC | principle components |
| PFR | plug flow reverser |
| PLS | partial least squares |
| PMR | Palladium Membrane Reactor |
| ppm | part per million |
| psi | pounds per square inch |
| RGA | residual gas analyzer |
| S:N | signal to noise |
| SRNL | Savannah River National Laboratory |
| SRS | Savannah River Site (Aiken, SC) |
| SSFM | stainless steel flow mount |
| T₂ | tritium |

1.0 INTRODUCTION AND BACKGROUND

Since the late 1970's, high resolution mass spectrometry has been the primary analytical tool used for hydrogen isotope analysis at the Savannah River Site (SRS) Tritium Facilities as well as throughout the DOE Weapons Complex. This analytical tool is used for material acceptance, product certification, surveillance, and safety. In 2001, a white paper by C. B. Mauldin and C.B. Gregory[1] outlined the problem of the aging mass spectrometers and associated risks to the Tritium Facilities at the SRS. Not only was the age of the instrumentation a concern, but the only supplier of these instruments had ceased production of them and intended to phase out support of existing instruments over a 10 year period with no guarantee that parts would be available over that same time period. To mitigate these risks, Mauldin and Gregory proposed a short term and long term strategic plan. The short term plan was to buy one of the last instruments to be made by the supplier and enough spare parts to maintain the instrument for approximately 10 years. This short term plan has been implemented[2] The long term plan consisted of three options: (1) redesign the electronics of the existing mass spectrometers to extend the life, (2) evaluate alternate commercially available mass spectrometers as replacement for the existing mass spectrometers or develop vendors to supply a replacement mass spectrometer, and (3) evaluate alternate technologies for hydrogen isotope analysis. In 2003, the same problem and risks were identified complex wide in a report from the Network of Senior Scientists and Engineers (NSSE) Advanced Technology Assessment Team (ATAT)[3] that summarized the gas sampling and analysis capabilities and needs at each of the DOE weapons complex sites, their long term viability, and the various technologies being pursued to maintain these analytical capabilities.

In support of the long term strategic plan suggested by Mauldin and Gregory, the Analytical Development Section (ADS) of the Savannah River National Laboratory (SRNL) began a program to evaluate potential replacement mass spectrometers as well as alternative technologies for use in the SRS Tritium Facilities. The goal was to maintain or if possible to enhance the current analytical capabilities. The need for on-line process control and monitoring was identified in the Tritium Facilities. On line analysis, though not a complete replacement for a laboratory mass spectrometer, could alleviate the sample load and thus extend the life of the laboratory instrument. In addition, one of the greatest advantages of on line analysis is that smart decisions in real time can be made, potentially increasing the efficiency and cost effectiveness of the process. Technological advances in miniaturization and high speed electronics has made on line measurements more practical. The analytical requirements for the control and monitoring of processes in the Tritium Facilities varies and in several cases do not require the use of a high resolution mass spectrometer.

This report summarizes the evaluation of

- a FT-ICR mass spectrometer
- a bench top magnetic sector mass spectrometer
- fiber optic Raman spectroscopy
- vapo-chromic sensors
- miniature infrared sensors

as alternative technologies to the high resolution laboratory mass spectrometer currently used in the Tritium Facilities.

This page intentionally left blank.

2.0 MASS SPECTROMETER

2.1 Introduction

The Siemens Quanta Fourier Transform Ion Cyclotron Resonance mass spectrometer (FT-ICR) and the JEOL GCMATE II compact, magnetic sector gas chromatograph mass spectrometer system were identified for evaluation as potential replacements or complements to the existing Tritium Facilities high resolution mass spectrometers. They are both small enough to be used in multiple process locations and cost between \$100 and \$200K, approximately one tenth the cost and one fourth the size of a conventional high resolution gas mass spectrometer..

Table 1 lists commonly found hydrogen and helium isotopes of interest and their mass to charge ratio while Table 2 lists the resolution required by a mass spectrometer to separate some of these ion pairs. Table 3 lists other light gases of interest for process control in the Tritium Facilities. The species in Table 3 are of interest since all of them can form from interactions of water, air, and organic materials in the presence of radiation. Note that high resolution is needed to separate common masses. For example, a conventional residual gas analyzer or quadrupole mass spectrometer, both of which have unit resolution, will not separate helium-4 from deuterium, methane from oxygen, hydroxyl from ammonia, carbon monoxide from nitrogen or nitrous oxide from carbon dioxide. The high resolution Finnigan mass spectrometer, currently used in the Tritium Facilities, has a resolution of 2800 at mass 28 and can separate most of the ions listed in Tables 1-3.

Table 1 Hydrogen and helium isotopic masses.

| Species | M/z |
|------------------------|----------|
| H+ | 1.007277 |
| | |
| D+ | 2.014102 |
| H₂+ | 2.01565 |
| | |
| ³He+ | 3.01603 |
| T+ | 3.01605 |
| HD+ | 3.021825 |
| H₃+ | 3.023475 |
| | |
| ⁴He+ | 4.002603 |
| HT+ | 4.023875 |
| D₂+ | 4.028 |
| | |
| DT+ | 5.03005 |
| | |
| T₂+ | 6.032 |
| D₃+ | 6.042 |

Table 2 Resolution of Ion Pairs

| Pair | Resolution Required |
|--------------------|---------------------|
| $D^+ ; H_2$ | 1220 |
| | |
| ${}^3He^+ ; T^+$ | 150000 |
| | |
| $T^+ ; HD^+$ | 520 |
| | |
| $HT^+ ; D_2^+$ | 980 |
| | |
| ${}^4He^+ ; D_2^+$ | 160 |

Table 3 Common ions in light gas mixtures

| Species | M/z | Possible Source |
|------------------------------------|---------|--|
| O | 15.9949 | oxygen |
| NH₂ | 16.0186 | ammonia fragment |
| CH₄ | 16.0312 | methane |
| OH | 17.0027 | hydroxide -water fragment, alcohols |
| NH₃ | 17.0265 | ammonia |
| H₂O | 18.0100 | water |
| NH₄ | 18.0350 | ammonium ion |
| Ar⁺⁺ | 19.9811 | argon |
| Ne | 19.9924 | neon |
| D₂O | 20.0229 | heavy water |
| Si | 27.9769 | from silanization or Si oxides, [sand is in all our samples from airborne dust - we work on top of sand hills; inside concrete structures] |
| CO | 27.9949 | carbon monoxide |
| N₂ | 28.0061 | nitrogen |
| C₂H₄ | 28.0313 | ethylene |
| N₂H | 29.0118 | protonated nitrogen - [common in ion traps] |
| C₂H₅ | 29.0390 | ethane organic fragment |
| NO | 29.9979 | nitrogen monoxide |
| C₂H₆ | 30.0468 | ethane |
| CH₂O | | aldehyde or alcohol fragment |
| Ar | 39.9623 | argon |
| C₃H₄ | | propane fragment |
| CO₂ | 43.9898 | carbon dioxide |
| N₂O | 44.0010 | nitrous oxide |
| C₂H₄O | 44.0260 | hydroxy ethanol |
| C₃H₈ | 44.0620 | propane |

2.2 Experimental

To evaluate the mass spectrometer systems, SRNL designed gas inlet systems and conducted tests using gases expected to be of interest to the Tritium Facilities as well as available samples from research & development programs within the SRNL. Gases used included hydrogen, deuterium, helium, nitrogen, and methane purchased from Air Liquide, Matheson, or Spectra Gases.

2.2.1 Siemens Quantra FT-ICR

Figure 1 shows a photograph of the Quantra system in SRNL. The Siemens Applied Automation division of Bartlesville, OK developed the Quantra mass spectrometer as a small FT-ICR system for on-line process monitoring in the petroleum industry. Sample is injected, via the piezo-electric injection valve, into the FT-ICR cell. Within the cell, an electron beam ionizes the sample. The ions formed are trapped by a magnetic field and charged trap plates and enter stable orbits at a cyclotron frequency that is dependent on the mass to charge ratio. A radio frequency signal resonant with the cyclotron frequency is applied which causes the ions to orbit with a larger radius within the cell. The receiver plates detect the signal from these orbiting ions and a fast Fourier Transform is performed to give the mass spectrum. A more detailed description of FT-ICR can be found in reference [4].

The Quantra system is unique in several ways. It uses a much smaller magnetic field generated by a non-cooled permanent 1 Tesla magnet when compared to larger FT-ICR systems which use 3 to 9 Tesla supercooled magnets. The weaker magnetic field lowers the cyclotron frequencies for a given mass and therefore lowers the radio frequency required by the instrument. For example, mass 2 requires a 30 MHz frequency with a 1 Tesla magnet but requires 100 MHz with a 5 Tesla magnet. However, the weaker magnetic field employed in the Quantra also limits the detection of higher masses to about 1000 amu. The instrument uses a picoliter piezo-electric injection valve in combination with a sealed vacuum system. Within the gold round cylinder labeled FT-ICR cell in Figure 1B, the vacuum system is maintained by an active ion pump which surrounds the small cylindrical ion trap located between the magnets. The SRNL Quantra system had two inlet valves, but the instrument supports adding a third inlet valve. The picoliter sample size is an advantage when working in a radioactive environment and the small sample size requirement also means that as an on-line process analyzer, sampling would not perturb the process stream. The sealed vacuum system eliminates the need for both an external pumping system (frees up valuable glovebox space in a radioactive environment) and exhaust of radioactive gases. However, eventually the ion pump would need to be regenerated or replaced. A limitation of the current Quantra system is that the electronics operating at 5 MHz limit the detectable low end mass to 12 amu if first order detection is used. Lower masses can be detected with less sensitive higher order harmonics and special tuning of the ion trap. The system has an ISA computer bus and uses a LINUX operating system with a small Pentium computer to drive a frequency generator and data acquisition cards.

Initially, experiments were performed by connecting a gas sample bottle directly to the piezo-electric valve capillary tubing on the Quantra. However, a more versatile inlet manifold allowed the mixing of gases, expansion of gas samples to look at the effect of various inlet pressures, and to perform static gas experiments (similar to pulling a gas sample from the process and taking it to a laboratory mass spectrometer) as well as flow through gas experiments (similar to an on-line measurement). The sample inlet system used in the evaluation was based on a design used by Quirinus Grindstaff on a developmental Quantra system that he acquired for use at the Y-12 National Security Complex. Figure 2 show details of the inlet system which incorporated digitally controlled pneumatic valving based on the Swagelok IGC II component manifolds. Two identical five port manifolds were used to couple the two piezo-electric inlet

flow-through valves on the Quantra to common manifolds. The manifolds were cross connected via the exhaust line and the piezo-electric valves, easily allowing gas expansion and flow through experiments. A MKS Baratron 390HA vacuum gauge was located on the inlet manifold and a Pfeiffer Vacuum PKR 251 combination cold cathode/Pirani vacuum gauge was located on the outlet manifold. A Pfeiffer Vacuum Turbo Drag pumping station (model TSH 071E) was used to evacuate the sample manifolds. The system has 4 sampling ports.

Figure 3 shows a screen capture of the sample inlet computer control interface and trending of the Baratron inlet pressure in real time. INA and INB are gas sample volume connection ports. Clicking with a mouse on the valve icon (dome shaped icon in Figure 3), opens the valve to the inlet manifold. Clicking on MSIN1 or MSIN2 lets the sample gas into one of the two piezo-electric capillary lines. MSOut1 and MSOUT2 can be closed for static gas measurements or opened for flow through gas measurements. The inlet and outlet manifolds can be connected by opening the valves and thus used for gas expansion to achieve various inlet pressures or for limited gas mixing. The inlet and outlet manifolds are evacuated through the exhaust line. National Instruments digital I/O relay lines provided 24 volt power to the pneumatic converters. A National Instruments ER-16 electronic relay control module was connected to a National Instruments 24 bit DIO card and was programmed with software using National Instruments Measurement Studio Active X components linked with Microsoft Visual Basic.NET. An alternative control scheme might have used a Siemens digital I/O card. However, their system did not have the full flexibility offered by independent programming.

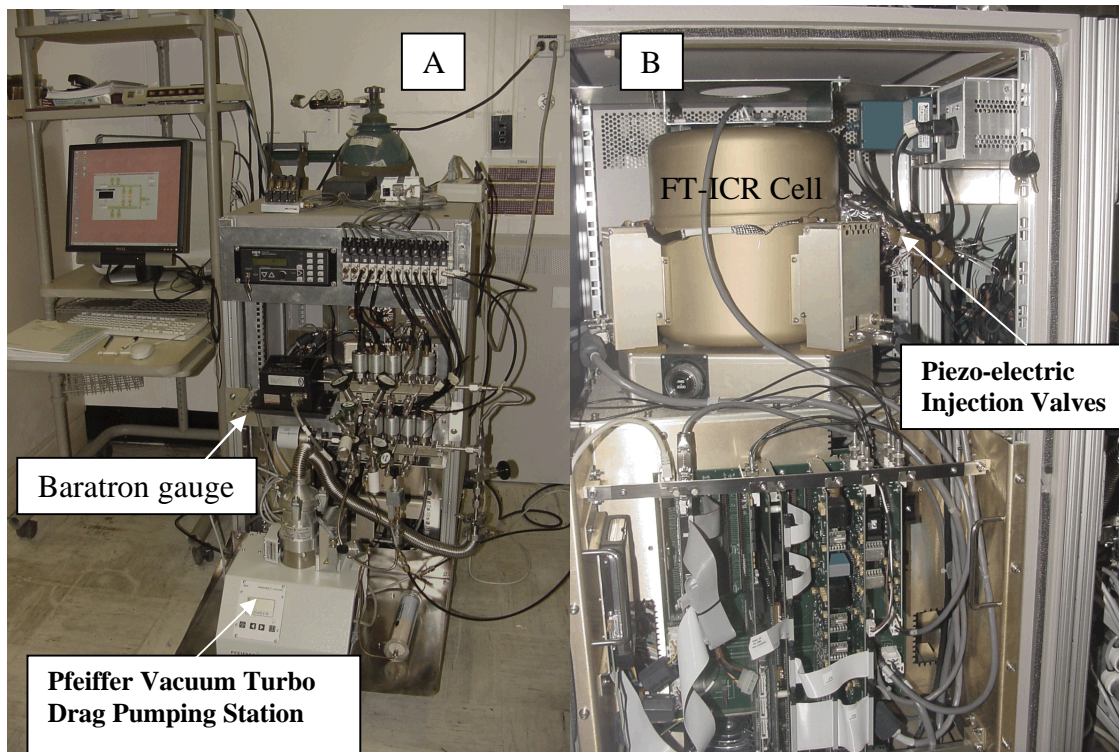


Figure 1 A) Siemens Applied Automation Quantra portable FT-ICR mass spectrometer with inlet system designed at SRNL. Dimensions are 42 inches high, 22 inches wide, and 24 inches deep. B) View inside the cabinet of the Quantra system. The FT-ICR cell is inside the round cylinder in the cabinet.

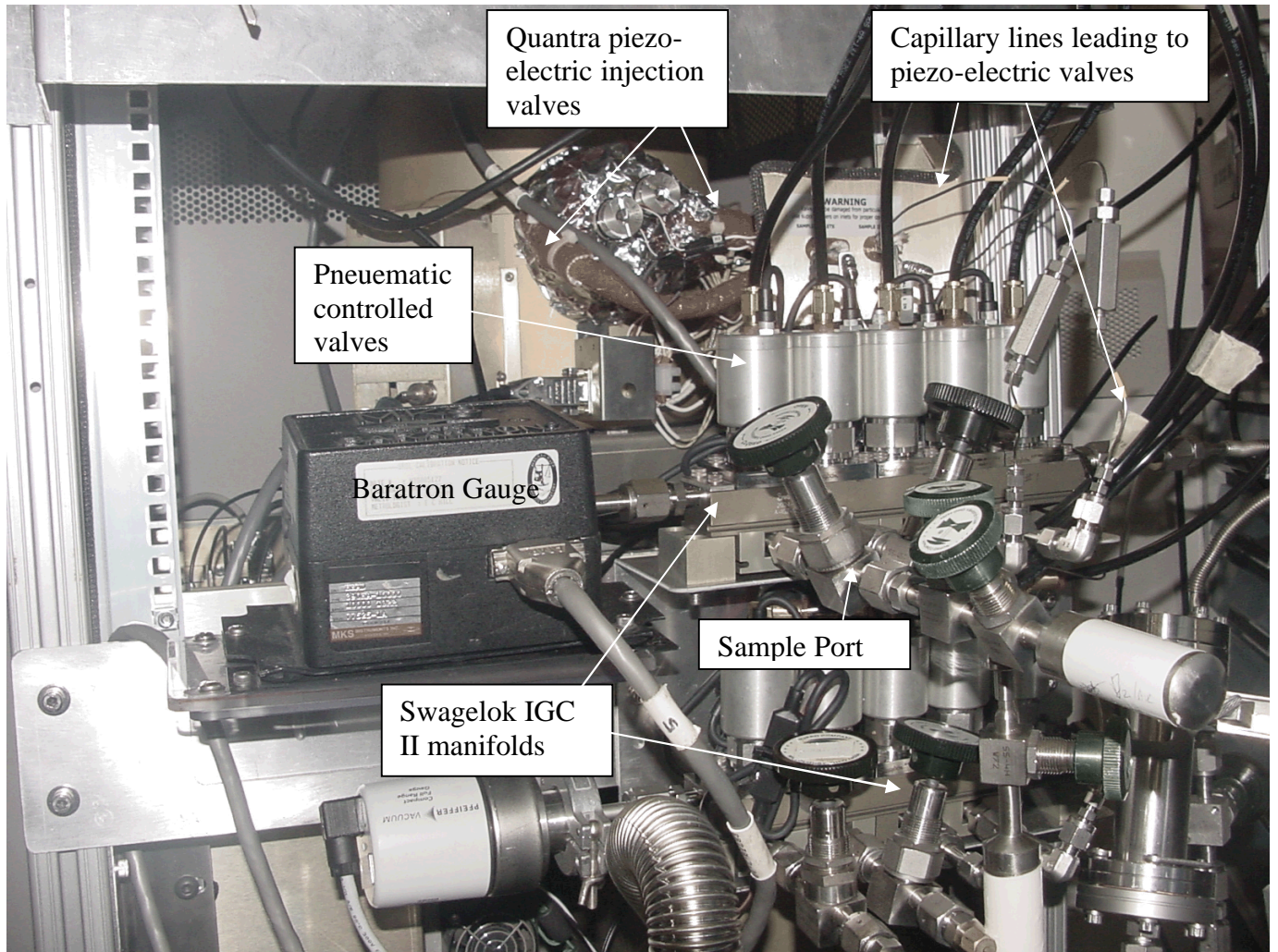


Figure 2 Sample inlet system for the Siemens Quantra using Swagelok IGC II manifolds and pneumatic controlled valves. The piezo-electric valves were heated and visible as the red lines in the photograph.

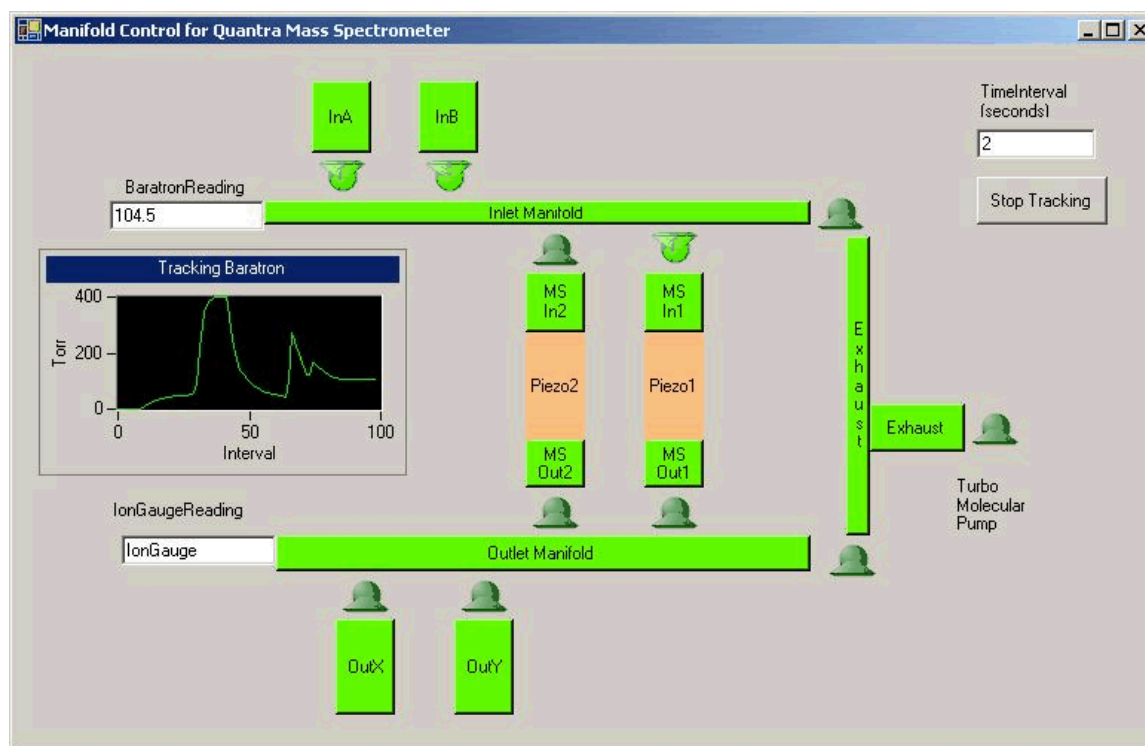


Figure 3 Sample inlet computer control and trending of the sample inlet pressure. Piezo1 and Piezo2 are the Quantra inlet valves.

Because the inlet and outlets were nearly identical, it was fairly straightforward to obtain a 50 percent reduction in inlet pressures by merely evacuating one side of the system and then expanding gas across the Quantra's piezo-electric one sixteenth inch stainless capillary lines. An approximately 10 percent reduction in pressure could be obtained by evacuating one of the piezo-electric lines and expanding into it across the manifold. Although the Quantra inlet system was designed to operate with a low pressure differential flow, we found that the system could operate well with static pressures from 1 Torr to 1000 Torr by adjusting the voltage on the piezo-electric valve to let into the system an appropriate number of ions. The Quantra internal ionization gauge behaved like a Penning gauge and its ion current, called the "isense" value, provided an indication of when an appropriate piezo-electric valve opening size was obtained and therefore, an appropriate number of ions injected for measurement. A limitation of the system was that at very low inlet pressures the isense value was masked by background noise levels within the ion pump. That is, the internal pressures of the trap are around 1×10^{-10} Torr and are at the limit for Penning type of measurements. In that case, we found that the actual mass spectrum analysis was more useful as an indication of ions in the trap.

2.2.2 JEOL GCMATE II Bench Top Magnetic Sector Mass Spectrometer

Figure 4 shows the JEOL GCMATE II gas chromatograph mass spectrometer (GC-MS) system. Figure 5 shows a photograph of the JEOL GCMATE ion source. This source is the key to this instrument and basically is a closed source design with very flexible ion focusing. The primary inlet is a capillary hole which allows gases from the gas chromatograph (GC) to directly reach the electron field inside the

source. The inlet is located on the side not shown. Small magnets are located about the filament to help contain the electrons and enhance ionization in the electron field. The entire source is held at a negative 2.5 KV below ground. The strong electric fields and the small magnetic confinement field help to keep the beam tightly focused and easily redirected using several stacks of lenses. The lens system includes right and left sides to allow slight sideways adjustments of the beam. Deflection plates allow the beam to be further bent for optimal alignment with the entrance slits into the first electrostatic filter section and then into the magnetic flight path and on to a second electrostatic section prior to detection. Two turbo pumps are used to maintain the system. The first is a large turbo molecular drag pump designed to rapidly move GC carrier gases such as helium from the source region. A smaller turbo pump is used after the first electrostatic entrance to provide higher vacuum for the flight path of the ions.

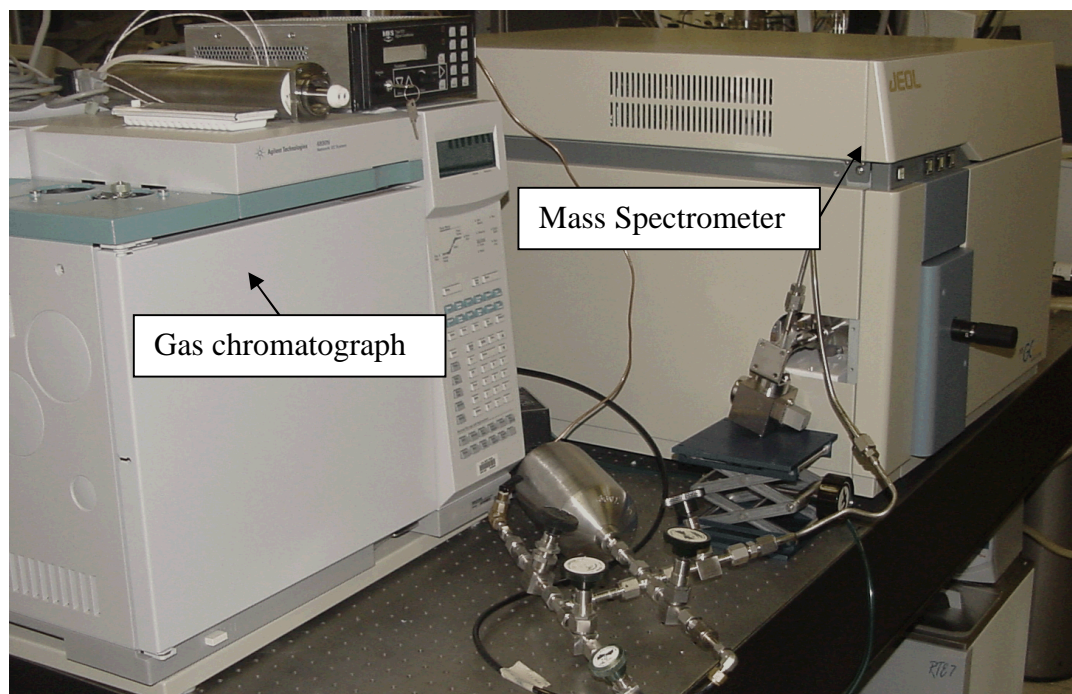


Figure 4 JEOL GCMATE II Gas Chromatography Mass Spectrometer System. The gas chromatograph has been removed from the inlet to the mass spectrometer for the evaluation studies.



Figure 5 JEOL GCMATE Ion Source

The system was installed in SRNL and the JEOL operating specifications were verified using the Agilent 6890 gas chromatographic (GC) inlet system. The system was calibrated to masses above 500 using perfluorokerosene. Resolution above 5900 was demonstrated for several test organic compounds. GC scanning operation and data acquisition was performed for full temperature scans up to 300 degrees Celsius.

To make the system similar to that used to feed the SRS gas mass spectrometers, the inlet system was modified to make it more of an open source design and be compatible for static rather than flowing samples in a carrier gas. Basically, we removed the capillary line and disconnected the Agilent GC. The flange, usually connected to the GC, was then tapped and connected to a Granville-Phillips variable molecular leak. A series of manual Nupro VCR valves were added to allow expansion of inlet gases into an evacuated one liter sample expansion volume. A simple diaphragm pump was used to evacuate these lines and the flask prior to introduction of sample gases from low pressure sample containers. A 1000 Torr MKS Baratron gauge was used to monitor system pressure. Figure 6 shows the initial gas inlet system for bench studies.

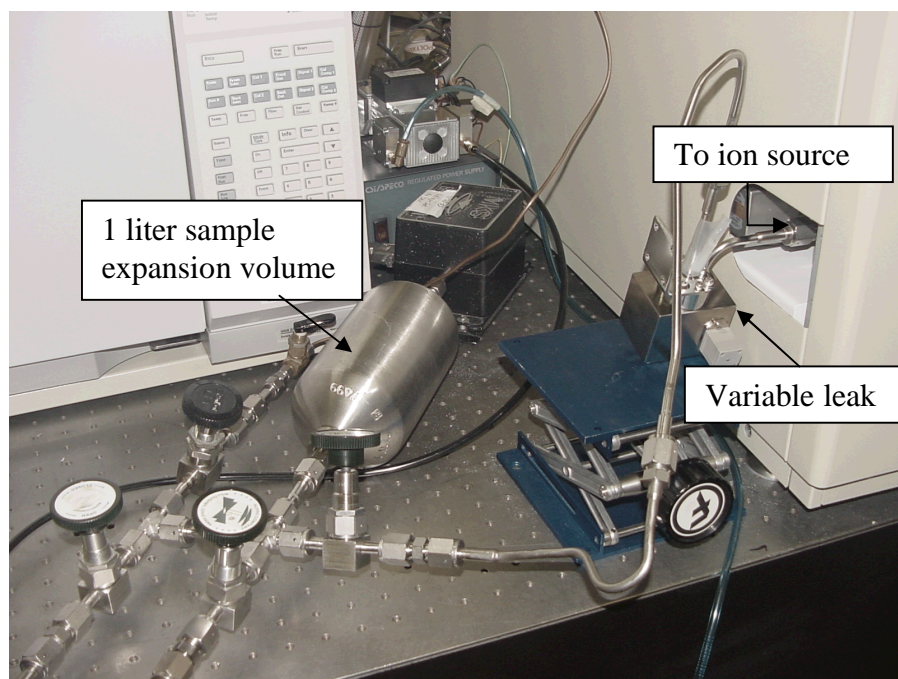


Figure 6 The initial test inlet system used a 1 liter sample expansion volume to lower inlet pressures and improve flow across the variable leak.

2.3 Results and Discussion

2.3.1 Evaluation of the Siemens Quantra FT-ICR

A significant advantage of an FT-ICR mass spectrometer is the phenomenal mass resolution that can be achieved with these systems. We were able to make use of this resolution during the course of the evaluation experiments to support ongoing radiolysis studies in the laboratory. Figure 7 shows the separation of carbon dioxide, nitrous oxide, and propane at mass 44. The resolution was better than 8900 using a Fast Fourier Transform (FFT) data set size of 521244. In a FT-ICR, increasing the data set size (parameter that is set in the software) for the transform improves the resolution. We found that the practical upper limit for the current version of the Quantra was a FFT data set size of about 2 million. This provided greater than 30,000 resolution at mass 28 (The Finnigan mass spectrometers currently used in the Tritium Facilities have a resolution of 2800 at mass 28). However, a trade off for increasing the data set size was that the ion lifetime in the trap had to increase. This means that as resolution improved, the number of ions that could be effectively maintained in the trap had to be decreased in order to avoid collisions and reactions that decrease the lifetime of an ion. If highly reactive ions and mixtures of ions were present, the total ion pressures had to be further decreased. A decrease in the number of ions in the trap results in a decrease in the dynamic range and a higher instrument detection limit.

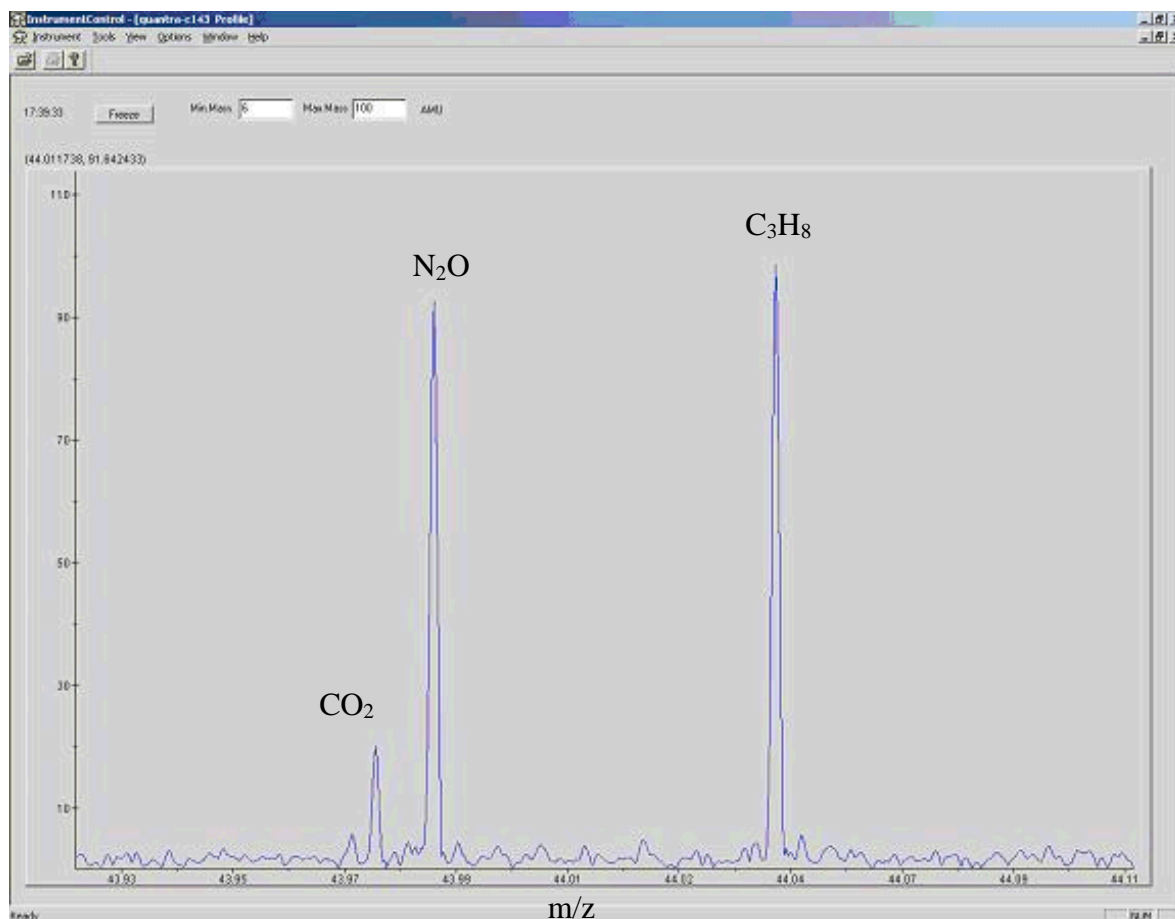


Figure 7 Carbon dioxide, nitrous oxide (N₂O), and propane(C₃H₈) could be separately analyzed. Mass calibration in this image is biased 0.02 amu low.

Figures 8 and 9 show the effect of ion ejection and data set size (resolution). Our system contained a small Teflon gasket that Siemens has since removed from their commercial systems. The gasket had low background levels of lubricant that would appear if the inlet valves were heated. Figure 8 shows the spectra of the system background with a minimal data set size of 8192. Figure 9 shows the same background taken with a data set size of 131288. Note the change in the peaks at masses 69, 119 and 170 as they become narrower as resolution increases.

Several issues were apparent when trying to do quantitative high resolution with the Quanta system. As mentioned the ion interactions and trap overloading had to be carefully matched to the data set size. Overloading and ion-ion interactions were not a severe problem with small data set sizes but readily apparent when reactive and poorly trapped ions were present. Samples with percent level concentrations of hydrogen readily interacted with nitrogen to form a hydride, N₂H ion at mass 29. If deuterium was present, the ion formed was at mass 30 as expected. This interaction could be prevented by lowering the inlet pressures but this would lower the overall dynamic range to only a couple of orders of magnitude. An alternative way to avoid ion-ion interactions was to use ion ejection to remove reactive and major ions. Removing all of the major ions allowed analysis in the hundreds of ppm range. For example, CO₂ in air (330 ppm) was readily detected by ejecting the nitrogen and oxygen peaks.

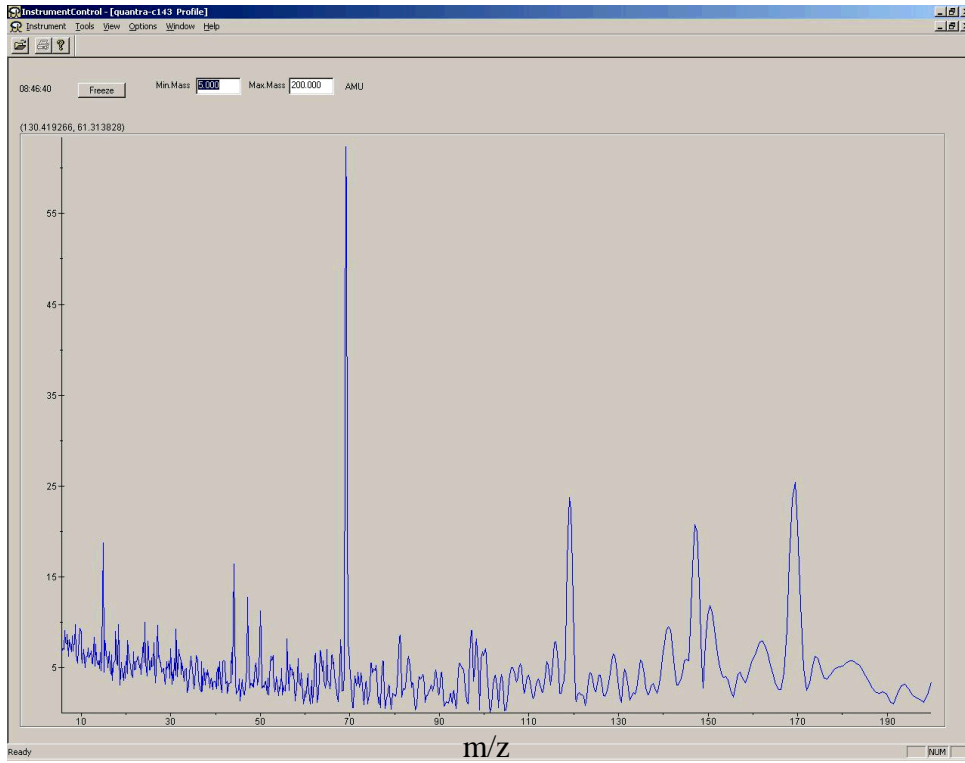


Figure 8 Background oil at low 8 K resolution. Major ions have been ejected.

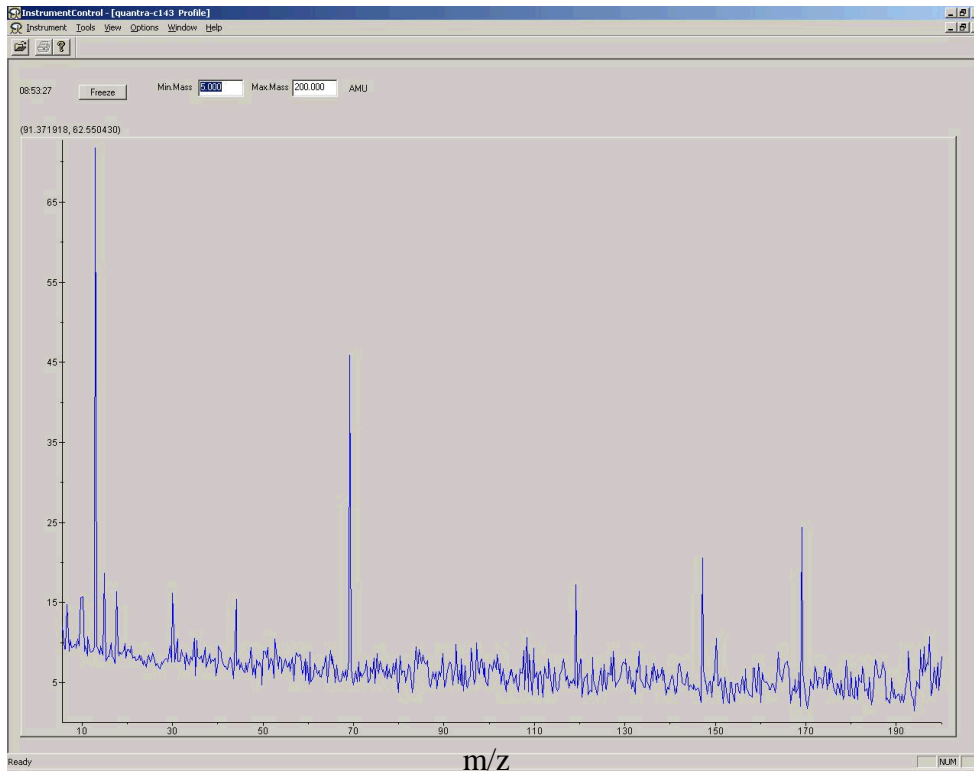


Figure 9 Background oils at high 131K resolution. Major ions have been ejected.

For use as an on-line process analyzer, the Quantra system would have to support multiple ion monitoring and data trending with repeated sample injections. Our experience indicated that the Siemens's software was easy to set up for monitoring selected masses that were different by 0.03 amu or greater, but that the fine adjustments needed to accurately trend ions closer in mass were difficult to attain. Figure 10 shows ion monitoring when a vial containing ammonia and methanol was repeatedly brought near the Quantra inlet that was constantly sampling the atmosphere. We were able to resolve and track the ^{16}O , [15.9949 amu from oxygen] from the methane fragment, [16.0312 amu]. Ammonia also was detected, but we found that we could not get the software to readily track the OH [17.0027 amu] from the NH_3 [17.0265 amu] even though the mass scans clearly showed that the two components were resolved and present at different concentrations. Siemens is aware of this problem and is expected to release a new generation of their software making it easier to set up and control measurements of ions at high resolution.

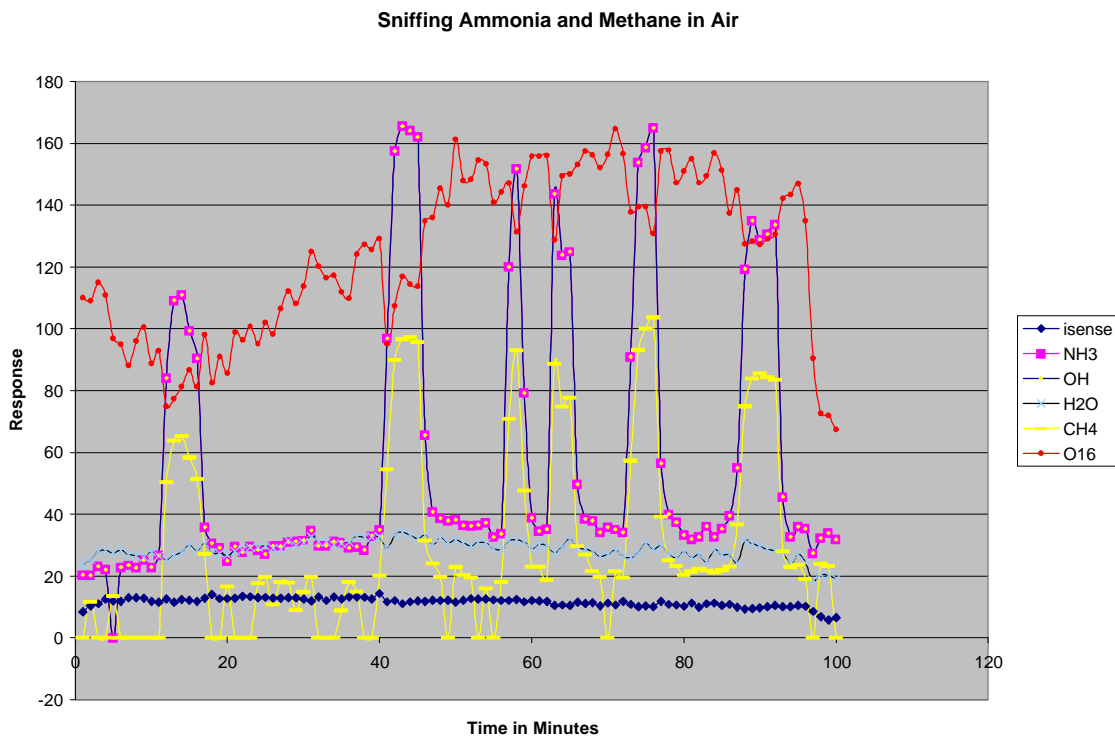


Figure 10 Sniffing ammonia and methane in air. Siemens software tracks ions in time but very close masses were difficult to setup to track independently. This examples shows ^{16}O and CH_4 were tracked but OH and ammonia were not. The isense value is a measure of the total internal ion current of the system.

2.3.2 Ion Trap Optimization and ionization current

Several studies were conducted to optimize the analysis conditions. Ion traps are extremely variable and must be tuned for each system. The orbit size, the trap beam voltage, and the trap excite voltages had to be optimized for best performance. Routines for these optimizations were part of the Siemens's software.

Figure 11 shows a plot of the filament current versus peak height. The peak height would generally increase to a plateau as the number of ions increased. However depending on the total ions available, the system could develop ion interactions and quenching. This is shown in the case of nitrogen in Figure 11. For analysis of major ions, the system optimized with a maximum current of only 60 nanoamps. However, in the case where major ions were ejected, the ionization current could be increased up to 1000 nanoamps. Detection limits in the parts per million range were possible by ejecting ions. We found this method useful for detecting trace organic vapors and carbon dioxide in air.

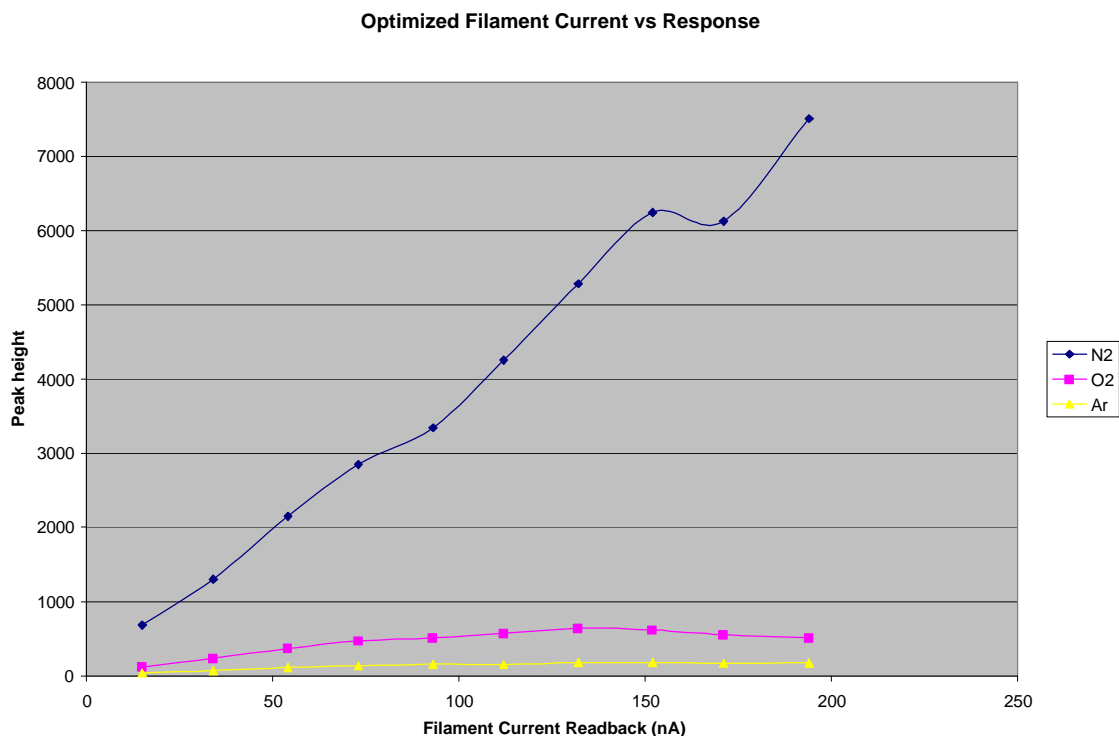


Figure 11 Filament Current Optimization

2.3.3 Helium and Deuterium on the Quantra

Although the minimum direct mass on the Quantra system is above 6 amu, hydrogen, helium, and deuterium can be detected by optimizing the trap to work at a third harmonic for hydrogen, and a second harmonic for helium and deuterium. Siemens provided a spreadsheet with a macro for calculating the expected frequencies for the harmonics. These are determined as beat frequencies against the 5 MHz fundamental frequency of the system. In our system, helium and deuterium appear around mass 9.35 after tuning the trap and excite voltage to double their normal values. We did several studies with helium and deuterium to determine the behavior of the system. These studies indicated that the detection sensitivity and range were in proportion to the ionization potential. Helium is difficult to ionize and had about one fourth of the sensitivity and range compared to deuterium which is relatively easily ionized. Figure 12 shows a plot of the response versus inlet pressure under set filament current and piezo-electric valve opening for deuterium and helium. Note that helium has much less of a detection range. Basically

the trap becomes overloaded with neutral ions as pressure increases. We noted that argon behaves similarly to helium. Although argon is more easily ionized than helium, it still is poorly pumped by the ion pump and the trap becomes overloaded.

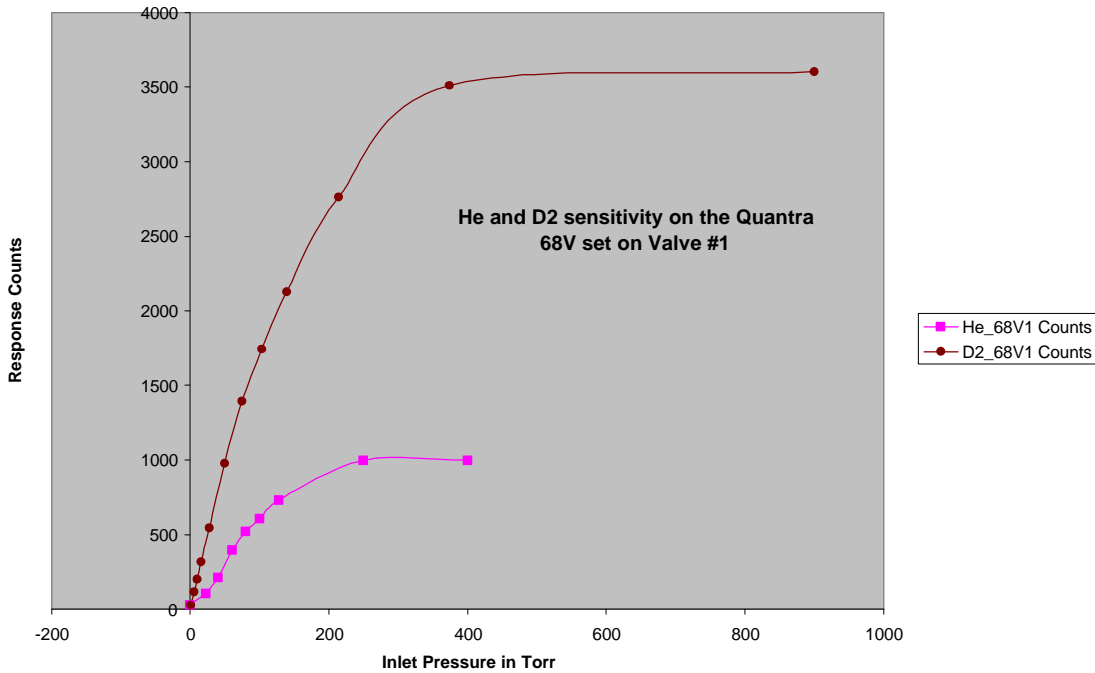


Figure 12 Inlet Pressure vs. Detection Saturation for Helium and Deuterium

Figure 13 shows a study with deuterium and the measurement of the isense value. Isense is the total internal ion current of the system and is limited by background and outgasing from the ion pump. A minimum isense value was between 5 and 7. The system optimized with an isense value of 15 which corresponded to an inlet pressure of between 50 and 100 Torr for a pure gas with an inlet piezo-electric valve opening set using 68 volts. Increasing and decreasing the inlet voltage allowed one to adjust the system pressure for optimum conditions.

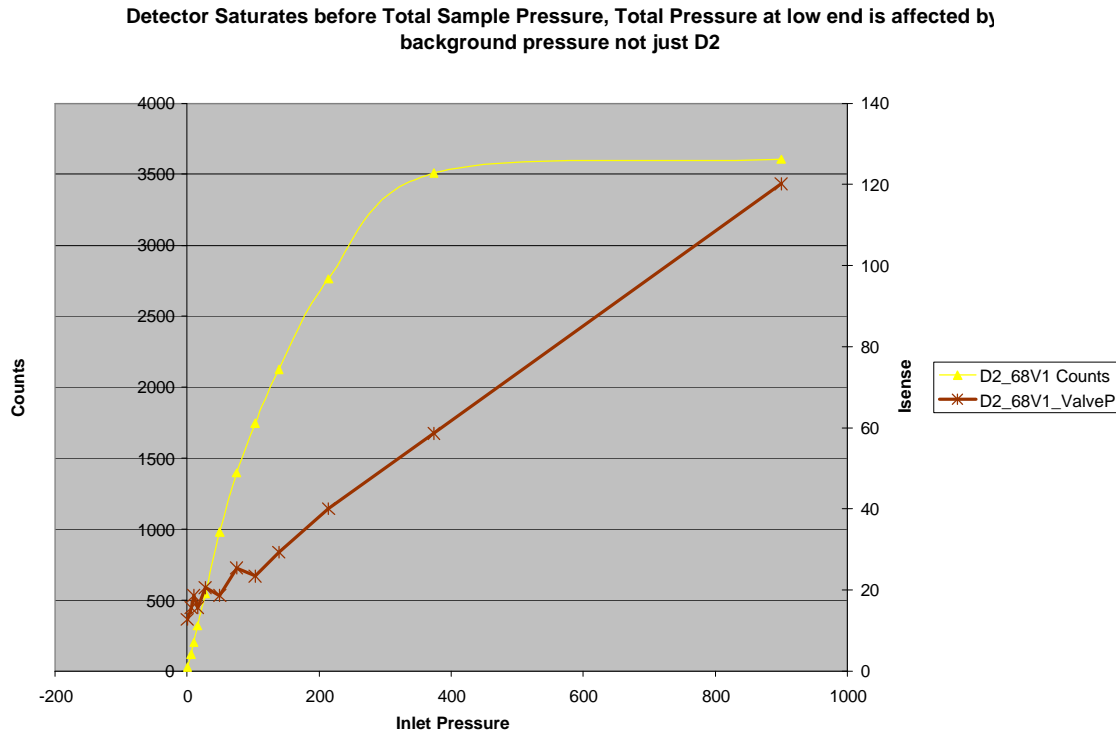


Figure 13 Detector and Isense Ranges

2.3.4 Evaluation of the JEOL GCMATE II Bench Top Magnetic Sector Mass Spectrometer

The JEOL GCMATE II system is a compact dual sector mass spectrometer that JEOL optimized for high resolution for GC mass spectrometry applications. The spectrometer system was designed primarily as a high end detector for a gas chromatograph.

Initial results indicate that the GCMATE has good sensitivity and can be tuned for analysis of hydrogen isotopes. Good separation of a He and D₂ mix was obtained as shown in Figure 14. Like the Quantra system, this system shows a significant bias in ionization efficiency for helium and deuterium implying that significant quantification factors will be required to appropriately scale results. Mass calibrations with the system appear to be stable for several days. Compromises in tuning need to be explored if both high [>20] and low [<4] mass ranges need to analyzed at the same time.

Several modifications to the initial setup will be made as we continue our evaluation of this mass spectrometer. A molecular drag pump will replace the initial vacuum pump to achieve lower pressures. Automated pneumatic valves will be added in addition to the manual valves. A crimped capillary will be used instead of the variable one.

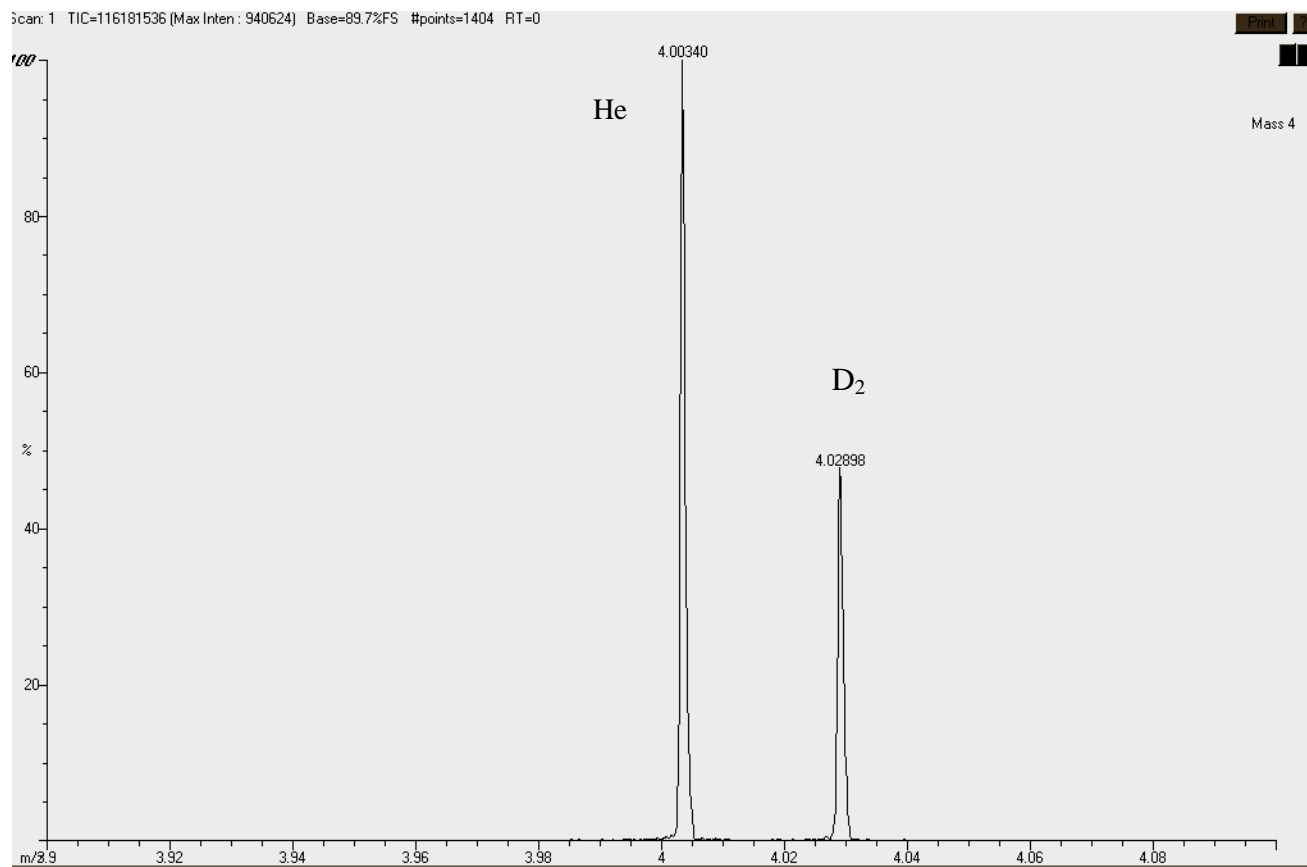


Figure 14 Helium and Deuterium separation using the GCMATE II. The resolution is 4100.

2.4 Conclusions and Recommendations

In its current configuration, the FT-ICR (Quantra) can measure masses 12 or greater, with a resolution of 30,000 at mass 28. Thus, the 16-24 mass region that is not so easily separated by the existing Tritium Facility mass spectrometers, could be easily resolved and measured using the FT-ICR. The instrument operates well at external pressures of 1 torr – 1000 torr and therefore could be directly interfaced to a process line for on-line real time analysis. The dynamic range and detection limits are affected primarily by overloading of the FT-ICR cell and ion-ion interactions within the cell. These factors are controlled by optimizing the voltage that controls the piezo-electric valve (thus limiting and optimizing the number of ions in the cell) and by utilizing the ion ejection capability. A detection limit of 100 part per million can be obtained using ion ejection of major ions. Work should begin on implementation of the FT-ICR (Quantra) as a complement to the existing mass spectrometers or as an on-line process analyzer.

For the FT-ICR (Quantra) to be of even more benefit to the Tritium Facilities, it should be re-engineered to provide analysis of masses 2-1000 in a single scan as well as other hardware and software improvements identified during our evaluation (i.e. improved mass stability for ion monitoring, quantitative analysis of mixtures, etc.). SRS, LANL, and Y12 have secured funding for this project and the re-engineering effort will begin in FY06. Once the re-engineering effort is complete, funding will be required for performance testing and implementation in a tritiated environment as well as validation for the design agency.

The GCMATE technology closely matches that of the existing mass spectrometers in the Tritium Facilities. The initial work with the GCMATE indicates that resolution and sensitivity meet the requirements of a replacement mass spectrometer for the Tritium Facilities. Although this instrument appears to be the most promising as a replacement for the existing mass spectrometers, delayed funding in FY05 precluded a complete evaluation. Therefore, evaluation of this instrument with a comparison to the performance specifications of the existing Finnigan mass spectrometers in the Tritium Facilities will continue in FY06 with ADAPT funding.

3.0 Fiber Optic Raman Spectroscopy

3.1 Introduction

Raman spectroscopy has been successfully demonstrated for the measurement of hydrogen isotopes.[5,6,7] However, by coupling Raman with fiber-optics, measurement of hydrogen isotopes can be performed quickly *in-situ* allowing fast adjustments of process controls to obtain the desired final product. We had proposed to interface and optimize a fiber-optic Raman probe and demonstrate it in the hydrogen-tritium thermal cycling absorption process (HT-TCAP). The challenges in this project included interfacing the probe to the production process (within a glovebox environment) and being able to measure the isotopes as they were cycled quickly in a high pressure environment.

Raman spectroscopy is a complementary technique to mass spectrometry, with several distinct advantages. Raman can simultaneously measure all the hydrogen isotopes and every isotope is readily resolved. Current high resolution mass spectrometer systems cannot directly measure all of the hydrogen isotopes. Because Raman can be coupled with fiber-optics, samples can be measured *in-situ*, with no need to pull samples off-line. The sample remains in its environment, undisturbed and intact, with no need for pressure reduction or long lengths of capillary tubing. As with mass spectrometry, very small sample volumes are needed and the resulting spectra are easy to interpret. The system needed for the Raman measurements is generally smaller and less expensive than most commercially available mass spectrometer systems.

Raman does however have its disadvantages. Generally, the detection limits for Raman are slightly higher than mass spectrometry. The signal is weak, as only 0.00001% of incident photons will be Raman scattered. While the signal can be improved with longer exposure times or higher laser powers, the advantages of quick measurements using small, simple and less expensive equipment will be quickly lost. Also, fluorescence from the sample or fiber-optics can obscure the Raman signal in some parts of the spectrum. This effect does not hinder the application described in this report as the vibrational shifts of hydrogen isotopes are well separated from the fluorescence regions. Another disadvantage is that any monatomic species, such as helium, a species of interest in the Tritium Facilities, cannot be measured by the Raman technique. Despite these disadvantages, Raman is a viable technique since it will meet the detection limit requirements for most processes and reduce the sample load on the older instruments, while analyzing for the hydrogen isotopes *in-situ*.

Some of the early hydrogen isotope analysis using Raman spectroscopy demonstrated the ability to monitor reaction kinetics. The Material Science and Technology Division in the Tritium group at Los Alamos National Laboratory, along with a research group from the Japanese Atomic Energy Research Institute, designed a 4 cm³ flow through cell for near-real time observation of hydrogen mixes.[8,9] They were able to analyze the isotopes in less than two minutes, with detection limits of 0.02%. They also determined the first order time constants for hydrogen isotopic exchange rates.[8,9] Uda and coworkers[10] used Raman to analyze isotopic methanes in fusion fuel gas processing systems. In addition to a flow cell, they used fiber-optics to deliver the laser energy to the cell. They were able to achieve a detection limit of 0.5% for hydrogen and methane. Engelmann and coworkers[11] used an ultra high vacuum tight stainless steel gas cell with very high quality silica windows to investigate the radiochemical reactions between methane and tritium. Mass spectrometry was combined with the laser Raman to create “a powerful combination of techniques for qualitative and quantitative analysis”.[11] Despite the successful analysis of the hydrogen isotopes, all of these efforts involve the use of an external

gas cell, which is not compatible with the hydrogen separation process in the Tritium Facilities.

The study of fiber-optics and probes for *in-situ* Raman analysis has been carried out over the years by many different research groups.[12,13,14,15,16] At SRS, remote chemical analysis using the Raman technique has been explored by Nave and coworkers.[17,18] This work used a rugged diffuse reflectance 6-around-1 probe. The fibers were angled to achieve a better acceptance angle for reflected light. This probe was used in conjunction with a pressurized sample system. The 1-1/8 inch diameter bore stainless steel pressure cylinder had a motorized linear actuator to compress gas in a sample cell to pressures of 500 psi. A detection limit of 0.1% hydrogen was observed. Malstrom also performed a study that compared and cross-validated Raman spectroscopy and real-time mass spectrometry for the analysis of hydrogen isotopes.[19] Although these studies worked quite well, they did not have the simplicity of a simple fiber-optic probe for measurement.

To show the benefits of the fiber-optic Raman probe for hydrogen isotope analysis, it was demonstrated on the HT-TCAP process. HT-TCAP is used to separate hydrogen isotopes, semi-continuously. A detailed description of how the HT-TCAP functions can be found elsewhere.[20] Separation of the isotopes is achieved by moving feed gas between a Pd/kieselguhr (catalyst) column and a plug flow reverser (PFR). The gas is moved by thermal cycling of the Pd/k column. Absorption of the gas from the PFR onto the cold column creates an isotopic concentration gradient in the column (-50 degrees Celsius). Desorption of the gas from the hot column back to the PFR only partially reverses the gradient (150 degrees Celsius). A steady state gradient is established after several cycles and a small fraction of the heavy and light isotopes are removed from each cycle.

For this demonstration, the Raman probe was positioned at the column midpoint. At this point, a pre-determined amount of feed is placed in the middle of the column and after cycling, product and raffinate are withdrawn from opposite ends of the column. The midpoint determines what proportion of the gas is withdrawn to the product and raffinate for the next cycle. Requirements for the midpoint testing were that the system must be able to sample at the end of the hot cycle when the column is filling and as it begins to cool, every 40 minutes. At this sampling point, the concentration of gases should be less than 5% D₂, greater than or equal to 95% H₂ and some HD. The pressure will range from 2500-3000 torr (\pm 500 torr) with a temperature of about 135 degrees Celsius. For HT-TCAP cold run testing purposes, H₂ and D₂ were separated. This separation gave critical process information for the eventual hot run tests using H₂ and tritium.

The primary purpose of the cold runs was to determine if the process was working correctly. Three different tests using different ratios of feed gas were fed into the column and separated accordingly. Those compositions consist of a 50:50 mix D₂:H₂, a 5:95 mix D₂:H₂, and a 20:80 mix D₂:H₂. The Tritium Facility also utilized a residual gas analyzer (RGA) to determine the composition of the mixes for these tests, measured at the midpoint, product and raffinate ends. Periodically, samples were also pulled and sent to the laboratory mass spectrometer, a Finnigan MAT 271, to verify the RGA readings. The Raman probe method, originally implemented solely for demonstration purposes, used the RGA and laboratory mass spectrometer measurements as its verification.

3.2 Experimental

A schematic of the Raman system used is depicted in Figure 15. This system consists of a laser (a), spectrometer and charge coupled device (CCD) detector (b), probe (c, d) and computer for data acquisition. The laser system (Figure 15a), Sapphire 200-488 CW (Coherent Laser Group, Santa Clara, CA), emits at 488 nm with the power ranging from 25 mW to 200 mW. This laser system consists of four parts: the laser head, heat sink for the laser head, control board and power supply. The laser is controlled via an RS-232 cable from the board by a computer program. Because the laser arrived in these separate parts, it was packaged into a boxed system measuring 12 inches long, 13.5 inches wide, and 8.5 inches tall (Figure 16a). This system is easily transportable, small enough to fit neatly on a two tiered cart and able to squeeze into tight spaces. A subminiature A (SMA) adapter was designed for the laser head so that the fiber-optic probe could be directly attached and the laser beam would be totally enclosed. This connection allows for anyone to operate the laser without being Class 4 laser trained. Another addition to the laser head was a 0.22 numerical aperture (NA) collimator, (World Precision Optics), to increase the amount of light entering the fiber. This collimator was placed on the laser head, before the fiber-optic, and allows 85% of the light to reach the end of the probe.

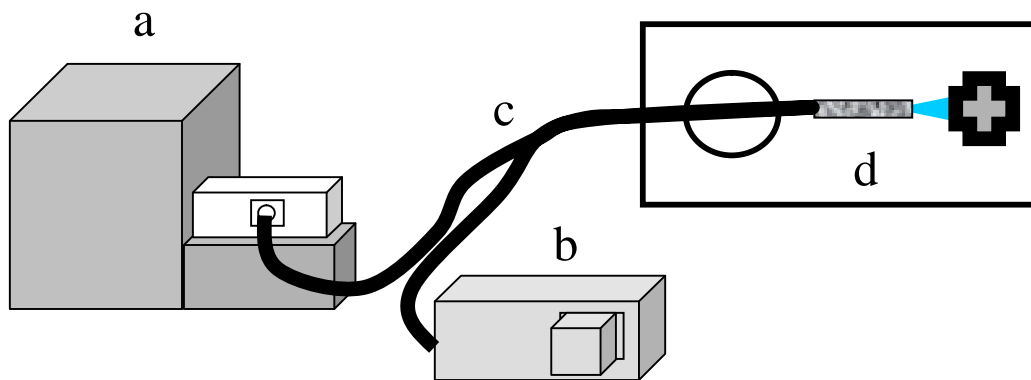


Figure 15 Schematic of fiber-optic laser Raman set-up;

Includes (a) 488 nm laser system measuring 12" x 13.5" x 8.5", (b) spectrograph, and CCD detector, (c) 20 ft. fiber optic probe, (d) fiber optic probe head inside glovebox.

A 20-foot fiber-optic probe (RoMack, Inc., Williamsburg, VA) was acquired, consisting of 6 collection fibers around 1 excitation fiber (Figure 16b). These fibers have a 400 micron diameter and a 0.22 NA. The common end, or detection end, consists of a ½ inch Swagelock VCR fitting for compatibility with the tee (cross) in the HT-TCAP line (Figure 16c). The fiber breaks out 17 feet from the common end into two separate ends: one excitation fiber to the laser head (Figure 16a) and six collection fibers to the spectrometer (Figure 16d). Both of these ends are terminated with a SMA connector and the entire fiber is jacketed with flexible stainless steel with a Teflon inner tube. The probe was designed to be 20 feet long to allow enough length in the glovebox for the probe to reach the detection tee and connect with the hardware outside of the glovebox. A push through fiber-optic grommet assembly (Douglas Electrical Components, Rockaway, NJ) with sealant was used at the glovebox port to bring the fiber-optic lines outside the glovebox, to the laser and spectrometer systems.

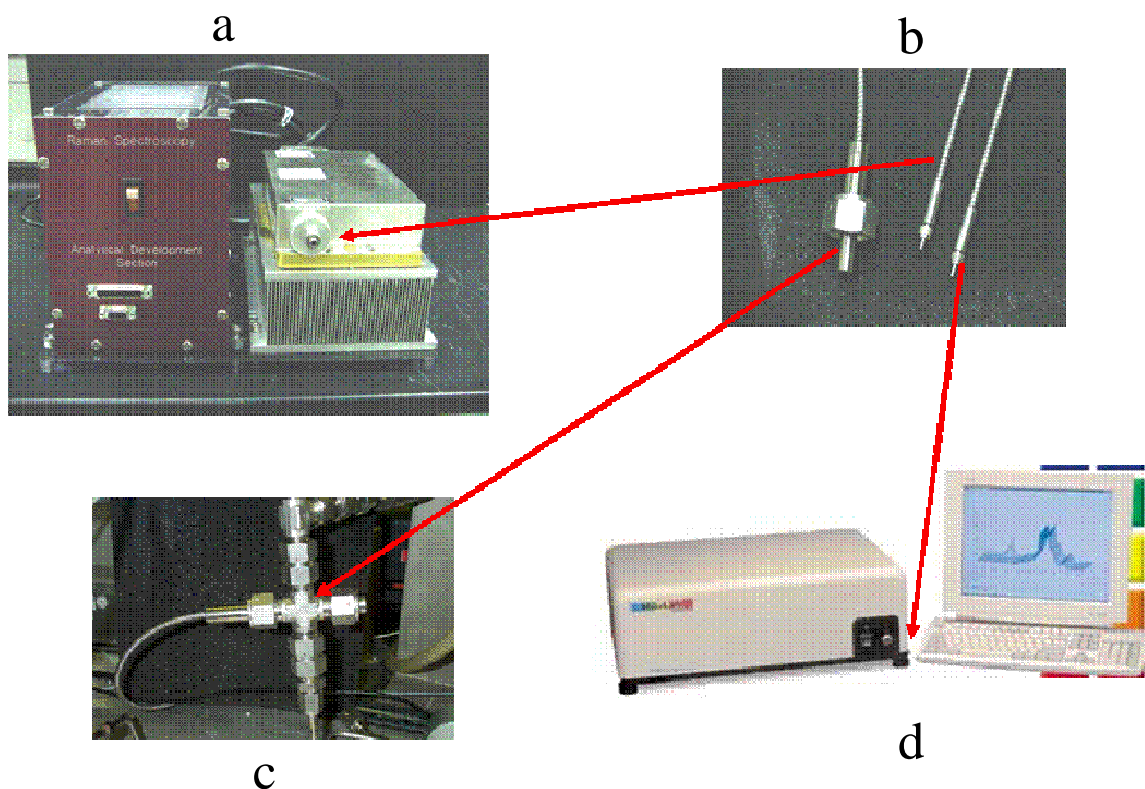


Figure 16 Raman System Components:

(a) Packaged laser system. Break away excitation fiber is connected to the laser head. (b) Fiber optic probe ends: common end (6 collection fibers around 1 excitation fiber) to plug into tee. Single ends (break away section of probe) to laser head (1 fiber) and to spectrometer (6 fibers). (c) Detection tee (inside glovebox) where common end is connected. (d) Spectrometer where break away collection fibers are connected.

Once the laser light was delivered to the tee and allowed to excite the gas molecules, the Raman signal was sent back down the fiber to a Kaiser Optical Systems, Inc., Holospec f/1.8 I VIS (Ann Arbor, MI) spectrometer (Figure 16d). The Holospec contains a 488 nm grating along with a SuperNotch-Plus 488 nm filter to block the laser light from entering the CCD detector. This DV-420-OE CCD detector system (Andor Technology, South Windsor, CT) consists of a 1024 X 256 pixel array. The system comes with Hologram software to control the detector and acquire data.

For the experiments, the laser was at its maximum power of 200 mW. Experimental data was acquired using various exposure times and either single accumulations or averaging several accumulations (exposures). The exposure time was the amount of time the detector was exposed to the Raman signal, while the accumulation was number of spectra captured during this time. If greater than one accumulation was selected, the exposures were averaged, producing one spectrum. Better signal to noise ratios were obtained using longer exposure times and a greater number of accumulations. There is however a trade off; as the exposure time and accumulations are increased, the signal to background improves, but the time it takes to collect the results rapidly increases. For example, the total amount of

time it takes for 1 spectrum to be collected using a 15 second exposure and 5 accumulations, is 150 seconds. Therefore, exposure times and accumulations were reduced depending on the analysis situation.

The region of 2700 cm^{-1} to 4300 cm^{-1} was the area of the spectra being interrogated. In this region, the rotational-vibrational transitions of the hydrogen isotopes are found. D_2 was found at a shift of 2971 cm^{-1} , HD was found at 3632 cm^{-1} , and H_2 shifted at 4132 cm^{-1} ³. For future investigations, T_2 can also be found in this region at a shift of 2466 cm^{-1} ³.

For data calculations, the operators needed the percent composition of the isotopes. First, a corrected signal intensity for the H_2 , D_2 and HD was calculated using the peak height for a given wavenumber and subtracting the average of the baseline on both sides of that peak. Ratios for the isotopes were calculated by comparing the corrected signal intensities to each other. This ratio is valid since the H_2 and D_2 cross sections are very close to each other. Percent composition was calculated using the corrected signal intensity for a given wavenumber divided by the sum of the H_2 , D_2 and HD corrected signal intensities. For process control, total H_2 and D_2 percent compositions were of interest. Assuming that HD was formed from equal amounts of the H_2 and D_2 , the measured percent composition of HD was divided and equal parts were added to the percent compositions of the H_2 and D_2 . Similarly, total H_2 and D_2 percent compositions were calculated from RGA measurements. Standard deviations (3σ) were calculated for 5 averaged spectra for all compositions and exposures. Detection limits were calculated as 3 times the standard deviation of a blank measurement divided by the slope of an intensity versus concentration plot.

3.3 Results and Discussion

3.3.1 Proof of Concept

For initial proof of concept in the laboratory, canisters of D_2 and H_2 were obtained at a 50:50 mix, 5:95 mix, 25:75 mix and 74:26 mix ($\text{D}_2:\text{H}_2$) and measured on a laboratory built gas manifold system. Total pressures of the mixtures were measured with a Sensotec pressure transducer placed at the detection tee. For each mixture, spectra were collected at various pressures, until the canister was emptied or a signal could no longer be discerned. Good signal-to-noise ratios could be seen in total pressures ranging from 11 to 4334 torr. A complete report of the laboratory testing can be found in a previous document.[21] The plots of signal versus total pressure for all the mixtures were linear yielding r^2 values of 0.999. Detection limit calculations were on the order of about 1% for D_2 and H_2 . With the proof of concept studies successfully completed, the fiber optic Raman probe was ready for demonstration during HT-TCAP cold run testing.

3.3.2 HT-TCAP DEMO

In late fall 2003, the HT-TCAP was ready to be tested. The Raman probe was placed at the midpoint in a tee. RGA gas transfer tubing was placed on the same tee directly across from the Raman probe for comparing results. The RGA tubing fed into a valve system on the glovebox port cover and was configured to sample various positions in the process. When the time came to sample at the midpoint, the HT-TCAP cycle was paused, the temperature and pressure would reach a semi-steady state (ramping of both would cease), and small sample volumes were pulled into capillary tubing for RGA analysis. For certain cycles, sample bombs were filled for laboratory mass spectrometry analysis. Sampling for the midpoint occurred at the end of the hot cycle before gas was pulled to the raffinate and product end and

before the cooling cycle began. The pause in the cycle allowed for a better comparison between the RGA and Raman because the same stream of gas was sampled.

The first cold runs performed were with a 50:50 mixture of $D_2:H_2$. A typical spectrum can be seen in Figure 17A. The probe head was placed on Column C at the midpoint. The D_2 peak is seen at 2994 cm^{-1} , the HD at 3632 cm^{-1} and the H_2 at 4155 cm^{-1} . The baseline in this spectrum is very noisy due to a light leak from the RGA tubing across from the probe head in the tee. Although most of this could be subtracted out, it still was a source of noise in the spectrum. In comparison, Figure 17B shows a 5:95 $D_2:H_2$ mixture where the probe was moved and positioned closer to the raffinate end, near the PFR. In this spectrum, the D_2 cannot be seen because its concentration is at the detection limit, about 1% for the Raman probe. In some cases, the HD began to reach the detection limit also.

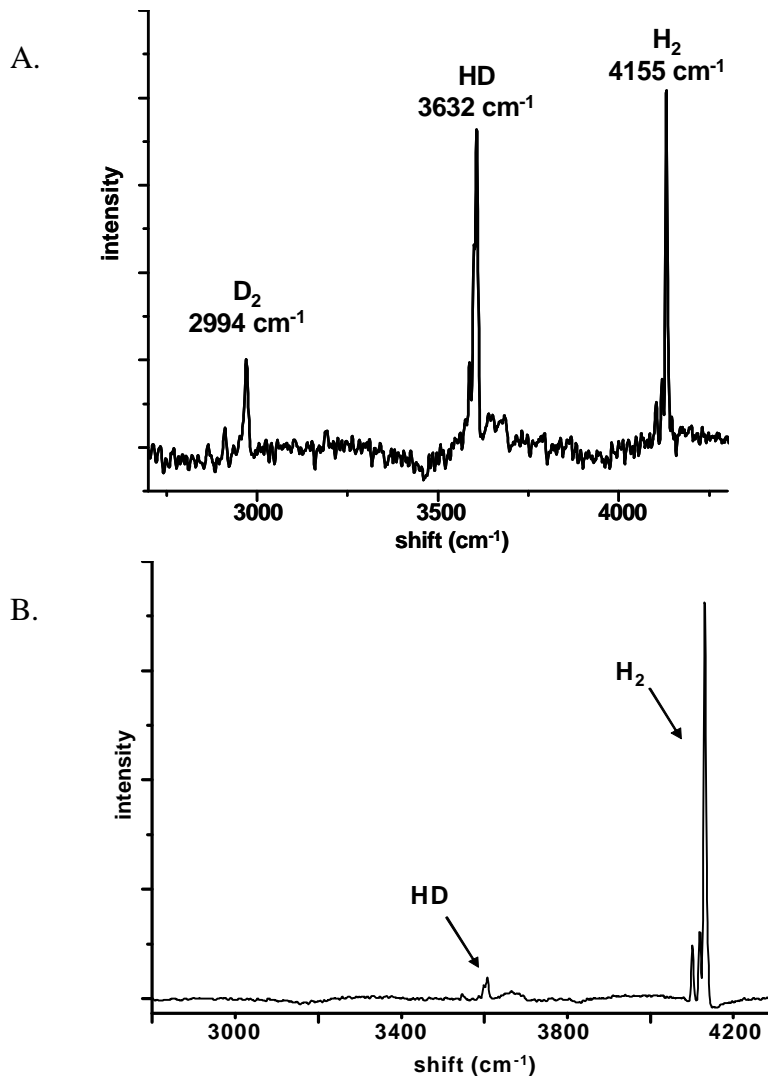


Figure 17 Typical Raman spectra from HT-TCAP cold runs. A. represents a 50:50 mixture at the midpoint. The baseline is choppy because of a light leak from the RGA sampling point across from the Raman probe head in the process tee. B. Represents a 5:95 mixture closer to the raffinate end. D_2 cannot be seen because the concentration is at the detection limit for the analysis.

Table 4 shows a comparison of typical results achieved by the Raman analysis and that of samples pulled for off line analysis by the mass spectrometer. The percent differences range from 3% to 6%. For process control, only total H₂ and D₂ were reported to the systems operators. Therefore, as stated previously, the amount of HD was equally divided among the H₂ and D₂. When this calculation was performed with the Raman data, the composition of D₂:H₂ was 34%:66%, a difference of about 3% from the laboratory mass spectrometer measurements at the midpoint.

Table 4 50:50 D₂:H₂ mixture results for the midpoint of column C. Results compare to those obtained by the on-line Raman analysis and the samples that were pulled for laboratory mass spectrometer measurements. Results agree to within 6% and discounting the HD, agree to within 3%.

| | Raman Results- On-line analysis | Lab MS Results | % diff |
|----------------------|--|-----------------------|---------------|
| D₂ | 13 % | 13.436 % | -3 % |
| HD | 41 % | 43.072 % | -5 % |
| H₂ | 46 % | 43.251 % | -6 % |

| Calculated Concentrations | Lab MS | Raman |
|--------------------------------------|-----------------------|--------------|
| D₂ | 34.972% • 35 % | 34 % |
| H₂ | 64.787 • 65 % | 66 % |

The 50:50 D₂:H₂ first round of testing was successful in providing operators with the information they desired. Therefore, for the next compositional cold run testing, 5:95 D₂:H₂, the probe was moved to a different position to aid operators with additional information needed. In this position, the probe was closer to the raffinate end and monitored the PFR exchange. Here, samples were pulled less frequently for off-line laboratory mass spectrometer analysis and so the RGA measurements were primarily used to verify the Raman results. Although the detection limit calculated for proof of concept testing was about 0.6-0.7%, this position and composition did prove to be more challenging. Table 5 shows results for both the end of the cold cycle and hot cycle testing. As seen here, the D₂ was indiscernible because the composition was below its detection limit, on the order of 1%. Therefore, there is a 100% difference between the Raman and mass spectrometry results for D₂. Similarly, the HD was almost at the limit of detection for the Raman system. Despite this, the ratios of total H₂ and D₂, the calculation of which includes the contributions from HD, were in agreement with the laboratory mass spectrometer results.

Because the HT-TCAP ran into various problems in the efficiency of its separation, the 5:95 D₂:H₂ mixture was cycled for several days. Table 6 shows results for several different cycles of both hot and

cold runs. Also shown in this table are comparisons of the Raman probe measurements with laboratory mass spectrometer results (when available) or RGA measurements. The data from the various methods are in good agreement with each other.

Table 5 Comparison of off-line analysis versus the Raman results for 5:95 D₂:H₂ mixtures. This data was taken from an area positioned closer to the raffinate end. The top chart represents the hot cycle (pressure of about 2000 torr) and the comparison between the lab mass spectrometer and Raman results. Again, D₂ was at its detection limit with the Raman therefore, it could not be seen. The bottom chart represents the beginning of the cold cycle (about 1400 torr of pressure) and the comparison of the RGA results and Raman results. Again, the limit of detection for D₂ is about 1% and the amount of D₂ at this position is much less than that. The HD measurements in both cases were reaching the detection limits as well, so the percent differences are much greater.

| Hot Cycle (2000 torr) | Raman results | Lab MS results | % diff |
|-----------------------------------|----------------------|-----------------------|---------------|
| D₂ | --- | 0.016 % | -100 % |
| HD | 2 % | 2.359 % | -15 % |
| H₂ | 98 % | 97.614 % | -0.4 % |
| Cold Cycle (1400 torr) | Raman Results | RGA Results | % diff |
| D₂ | --- | 0.16 % | -100 % |
| HD | 0.8 % | 0.71 % | -13 % |
| H₂ | 99 % | 99.13 % | -0.1 % |

Table 6 More comparison results for 5:95 D₂:H₂ mixtures. The probe was positioned closer to the raffinate end. The HD was reaching its detection limit while the D₂ was at its detection limit. Results are in good agreement between the RGA, lab mass spectrometer and Raman.

| | | | |
|------------------------|--------------|------------|---------------|
| Cycle 298- Hot | Raman | RGA | |
| D ₂ | --- | --- | |
| HD | 3 % | 2.53 % | |
| H ₂ | 97 % | 97.4 % | |
| Cycle 299- Hot | Raman | RGA | Lab MS |
| D ₂ | --- | --- | 0.016 % |
| HD | 2 % | 2.47 % | 2.359 % |
| H ₂ | 98 % | 97.53 % | 97.614 % |
| Cycle 306- Cold | Raman | RGA | |
| D ₂ | --- | 0.12 % | |
| HD | 2 % | 1.16 % | |
| H ₂ | 98 % | 98.72 % | |
| Cycle 320- Hot | Raman | RGA | |
| D ₂ | --- | 0.04 % | |
| HD | 2 % | 2.24 % | |
| H ₂ | 98 % | 97.72 % | |
| Cycle 321- Cold | Raman | RGA | |
| D ₂ | --- | 0.16 % | |
| HD | 2 % | 1.07 % | |
| H ₂ | 98 % | 98.78 % | |

The most significant advantage of the Raman system was that it allowed for continuous monitoring of gas passing the midpoint. Although the pause was placed in the cycle to stop for collection of data, it was truly not needed for the Raman analysis. Data could be collected for the entire heating cycle, as the pressure and temperature both steadily increased. Because the signal was so strong at these high temperatures and pressures, very short exposure times could be used. It was originally thought that longer exposure times would be needed to yield decent spectra however, the short exposure times allowed more data to be collected. Spectra could be collected every 3 seconds and the isotope exchange in the column could be viewed in real time.

Using HT-TCAP as a demonstration process allowed operators to see the power of Raman spectroscopy. A feature that is uncommon to isotope analysis in the facilities is the ability to continually monitor and analyze the isotopic separation throughout most of the entire HT-TCAP cycle. For instance, when the column is first heating up, the majority of the gas moving across the midpoint is D_2 . This is mainly because the column has an affinity for the H_2 and not the D_2 . As the column begins to heat up to higher temperatures, the H_2 is driven off. The only time that data could not be collected in the cycle was during the cooling of the column. During this time most of the gas had moved past the midpoint and into the PFR. Pressures and concentrations during the cold cycle were too low at the midpoint so no valuable information could be obtained using Raman. Data could be taken at the beginning of the cold cycle (before the drop in pressure) and throughout the hot cycle (ramping of the pressure). Figure 18 shows this data over time concept. Since the RGA required pulling a sample off-line for analysis, this same data shown in Figure 18 would have been practically impossible to have obtained with the mass spectrometer systems or the RGA since a very large number of samples would have needed to be taken.

For the 40:60 $D_2:H_2$ mixture, the probe was repositioned again. Because of process control issues and time constraints, the probe was placed outside of the glovebox and connected to the other end of a tee used for pulling RGA samples. The sample valves on the glovebox port were left open so that gas was continually flowing through the lines. Measurements were still occurring in real time, the probe was just not directly in the process. Again, data was in good agreement with the RGA and laboratory mass spectrometry results.

Figure 19 again shows one of the advantages of the online Raman technique. This graph plots the relative percent of both D_2 (♦) and H_2 (◻) over time (minutes) for an entire heating cycle. At the beginning of the cycle, the majority of the gas is D_2 (70%). As the column heats up, the H_2 passes by the midpoint on its way to the PFR. As the PFR is used to maintain an isotopic gradient, it makes sense that as the column cools, the gas leaves the PFR in the same profile that it entered so that in the beginning of the heating cycle, the concentration is high in D_2 . At the end of the heating cycle, before gas is sent to the raffinate and product beds, and when sampling is to occur, the composition of the H_2 is about 67% and that of the D_2 is 33% (not including the HD).

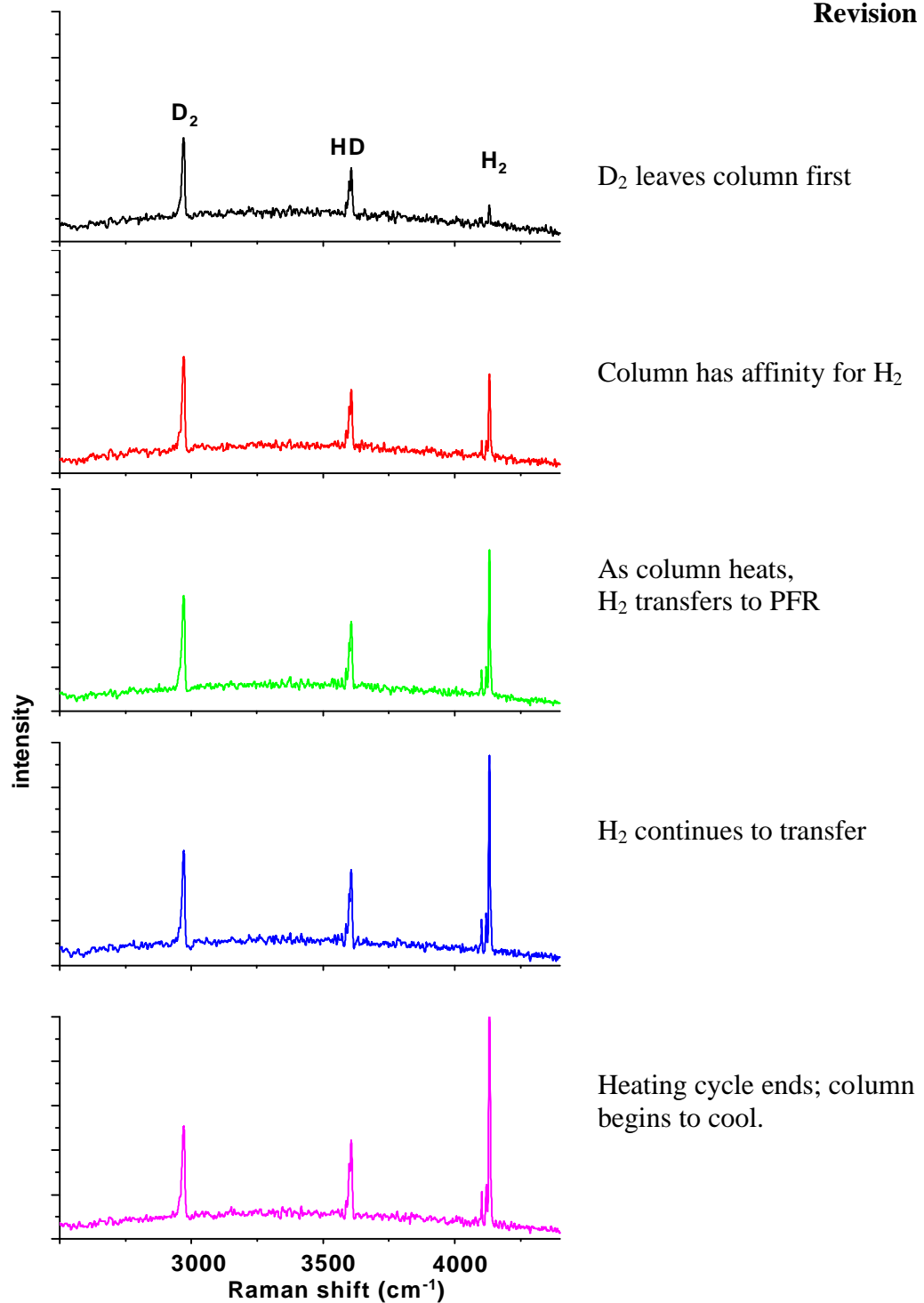


Figure 18 Real time measurement using Raman. This example of the 40:60 D₂:H₂ mixture shows that Raman can be used to watch the isotope sweep across the midpoint. As seen here, when the heating cycle begins, D₂ is most abundant at the midpoint. Because the column has an affinity for the H₂, it is slower to leave the column. As the heating cycle continues the H₂ is released. Over time, the H₂ continues to move down the column and that is the most abundant isotope seen at the midpoint.

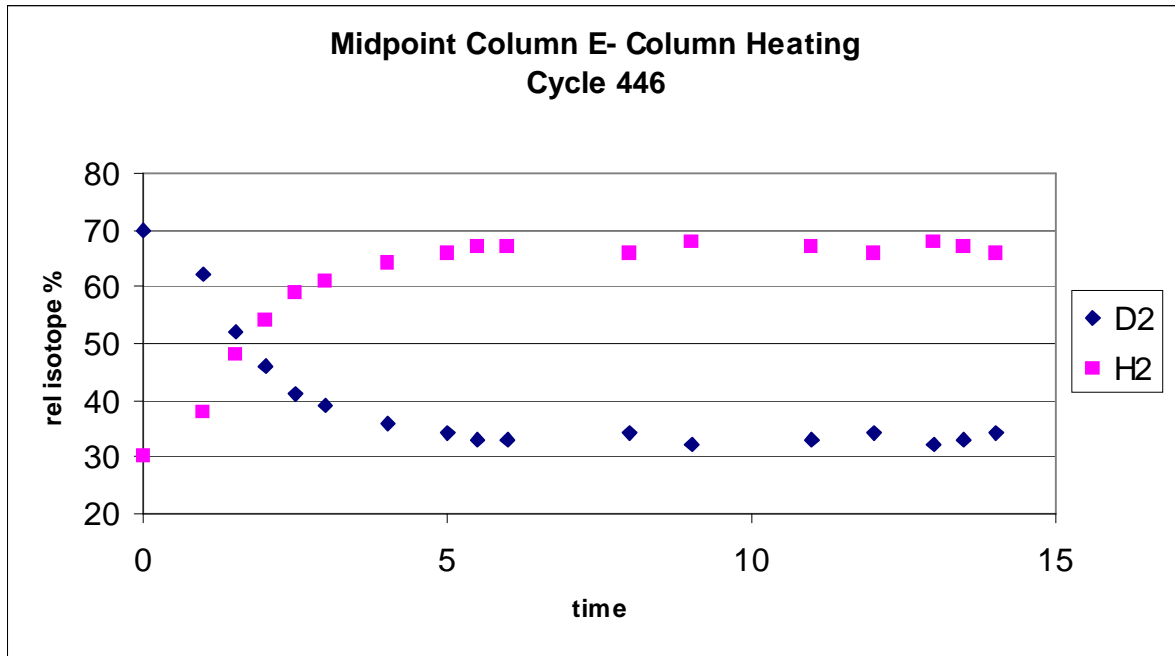


Figure 19 Cold Run testing for 40:60 D₂:H₂. Plot of % ratio of the isotopes versus time. At time 0, the hot cycle begins, and at time 15, the hot cycle ends and the cooling of the column begins. The relative percents at the ending point are 67% H₂ and 33% D₂. (HD was not calculated into these percentages but would be about the correct ratio if added to each of the H₂ and D₂.)

3.3.2.1 Advantages over RGA

Because the Raman system collected data in real time, operators were able to utilize this real time information to determine that the pause for sampling was in the incorrect point during the first set of HT-TCAP cycles. Incorrect placement of the pause for sampling caused the RGA detector to saturate because the sampling point pressure was too high. Because the detector saturated, the RGA at this point provided no useful information. The Raman system, since it wasn't dependent on the pause in order to take a sample, was able to continue to acquire data that was used to verify that the sampling pause was in the incorrect point in the cycle.

Gas analysis using the Raman method is non-intrusive whereas analysis with an RGA is intrusive to the process. With an RGA or any mass spectrometer, a sample of gas must be taken from the process for analysis. This leads to two issues: the first is that in order to sample the next cycle, the RGA line must be flushed to ensure that no contamination will occur from previous runs. The second issue is that the sample of gas cannot go back into the process, so it must be exhausted. Flushing lines and the exhaust of tritiated or any hazardous gas adds time to the analysis as well as the expense and glovebox space requirements of vacuum systems. With the Raman being in-line with the process, there is no need to flush sample lines and exhaust gases. The only possible problem that could occur would be if the probe was not sealed properly. Gas could leak into the probe head, down the fiber shielding and out of the glovebox. This was a concern to operators, therefore a probe with a brazed sapphire window has been obtained for tritium analyses. This probe, along with all probes placed within the glovebox, are pressure tested and leak tested.

3.3.2.2 Exchange Tests

During initial cold run studies, it was determined that the column was not properly separating the isotopes. A troubleshooting effort began to determine the cause of the improper separation and the Raman probe proved beneficial to the resolution of this issue. One of the tests needed was determining the rate at which the isotopes leave both the column and PFR. If the isotopes lingered and did not come off immediately, this could indicate a problem with the material used. Because the Raman could give real time results, specific tests to determine column hold-up were designed. Using Raman saved a lot of sampling and analysis time since the rate at which sampling was needed was fast and frequent. Using the RGA was virtually impossible because of the fast breakthrough times that would occur. A full report of these Raman troubleshooting efforts can be found in other documentation.[22,23]

3.3.2.3 Path forward

The benefits of fiber optic laser Raman spectroscopy were apparent during cold run testing in HT-TCAP. The path forward for this work includes several tasks. The first task, which has been completed, is automation of the system. Although data acquisition was relatively simple, the author was needed to perform the data calculations to obtain percentages. Since then, a program to automatically record the spectrum and transfer the data to a spreadsheet for percent isotope calculation has been created. This will allow operators to set up an experiment and have the system acquire the data and report the ratio of D₂:H₂. Second, although it has been shown by other groups that tritium analysis by Raman spectroscopy is possible, it has not been proven to provide acceptable results with a set-up as simplistic as that presented in this report. Because of the simplicity of the set-up, it would be advantageous to use the probe at various positions within the HT-TCAP process to provide real time information. It is possible to set-up multiple probes and have them all connect to one instrumental set-up. This would alleviate the need to pull samples for mass spectrometer analysis and would also provide instantaneous feedback without the need to wait for results and possibly have to rerun certain cycles and beds.

3.4 Conclusions and Recommendations

A fiber-optic Raman system was demonstrated in cold run testing of HT-TCAP for the analysis of hydrogen isotopes. The advantage of Raman is that it is able to discriminate between all forms of protonated, deuterated and tritiated species (i.e.HD, HT, TD, D₂, H₂ and T₂). This system was able to analyze for H₂ and D₂ at the specified pressures of the HT-TCAP column midpoint as well as other process locations. Three separate testing schemes were used and the probe demonstrated excellent correlation with RGA and mass spectrometry results in all the positions it was tested. Although the Raman probe detection limit was on the order of about 1%, higher than required for the product and raffinate, valuable information was obtained for the midpoint, which is especially needed for process control. It is possible to place several probe heads at different places in the process and multiplex these to a single detector. This would allow operators to take information when and where required without having to wait for mass spectrometry analysis. Placing probe heads at, for example, various feed bed locations, will prevent operators from having to re-run because of contamination or incorrect feed concentrations. Although, the authors have not tried this analysis with tritium, they feel confident that they will get acceptable results.

This page intentionally left blank.

4.0 VAPOCHROMIC SENSORS

4.1 Introduction and Background

Ammonia and moisture are two species that can negatively impact the efficiency of hydrogen processing. Thus, on-line, real time monitoring of these species would be beneficial. Most commercially available ammonia and moisture sensors rely on electrolytic permeable polymers for detection. These permeable polymers suffer from the lack of resolving power to differentiate between ammonia and moisture and rely on electrolytic measurements in a potentially explosive ($> 4\% \text{ H}_2$) environment. To overcome these limitations, researchers at SRNL have been collaborating with researchers at the University of Minnesota and the Center for Process Analytical Chemistry to employ fluorescence emission from inorganic complexes (vapochromes) to detect both vapor phase moisture and ammonia. These vapochromic crystals show both intensity changes and signature shifts in the fluorescence maximum after sorption of various gas phase analytes.

The investigation of new materials as potential transducers for optically-based vapor sensors is an active area of research.[24,25,26,27,28] Optically-based vapor sensors are numerous and have been used for the qualitative identification of pure solvent vapors and the quantitative determination of vapor concentrations. Many materials undergo useful optical transformations in the presence of various solvent vapors. The most commonly studied systems use a polymer matrix containing solvatochromic dye molecules[24]. The molecular origin of the sensing signal in these systems is the change in the optical properties of the doped dye molecule that results from changes in polymer matrix solvation.

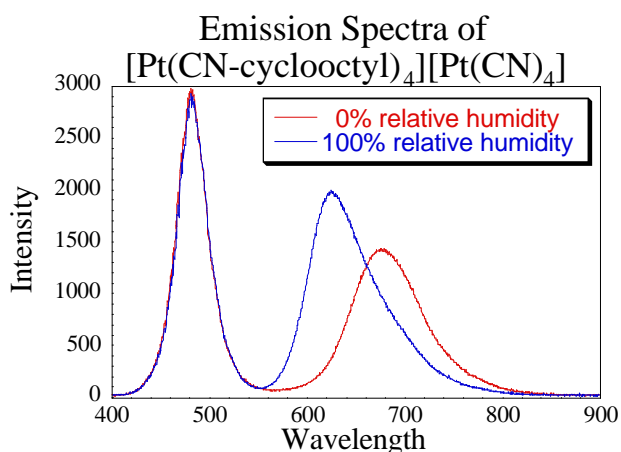


Figure 20 Emission profile of vapochrome compound in the presence of 0 and 100% relative humidity.

Analogous to the solvatochromic molecules, vapochromic materials directly sense solvent vapors by incorporating solvent vapors into the structure of the material[26,29,30]. The color of these materials is modulated by direct molecular interactions between the chromophore and the solvent vapor. The color change observed depends both on the identity and the concentration of the solvent vapor (Figure 20).

Vapochromism in crystalline salts arises from highly anisotropic packing forces that enable solvent vapors to reversibly penetrate the interior of the material to form a new crystalline phase with precisely determined solvent – chromophore interactions. These

include changes in the dielectric constant near the chromophore, hydrogen bonding between the solvent and coordinated cyanide, and expansion or contraction of the unit cell that is coupled to the Pt – Pt distance[29]. The vapochromic solids consist of infinite stacks of alternating $[\text{Pt}(\text{CNR})_4]^{2+}$ dications and $[\text{Pt}(\text{CN})_4]^{2-}$ dianions. Interionic metal – metal interactions produce the chromophore. The vapor inclusion causes the color changes that result from a combination of solvent – chromophore interactions mentioned previously.

For this work, several vapochromic compounds were evaluated for their response to vapor phase moisture and ammonia. The ideal candidates were then further tested against lower levels of ammonia (0.3 – 3%). A partial least squares (PLS) algorithm was utilized to evaluate the multivariate response to ammonia. Vapochromic compound screening, testing and multivariate data analysis will be discussed.

4.2 Experimental

4.2.1 Gas Generation System

Various concentrations of ammonia were delivered from lecture bottles (Scott Gas) after being diluted with dry nitrogen. Calibrated mass flow controllers (Aera 980C) were used to meter the flow of all gases during the experiments. The mass flow controllers were controlled via a laptop computer (Dell Inspiron D600) through RS232 communications ports. All gas lines were maintained at constant temperature inside an incubator where gas temperatures were verified upstream of the sensing system using a RTD.

4.2.2 Vapochromic Sensor Probe

A fiber optic reflectance probe was constructed for the measurement of vapor phase ammonia levels as shown in Figure 21. The probe was constructed using a commercial bifurcated fiber optic reflectance/backscattering probe (Ocean Optics, model R400-7) inserted into a modified stainless steel flow mount (SSFM) along with a 10-mm optical window coated with a vapochromic compound. The SSFM allowed both simple adjustment of the distance between the probe and coated lens and stable mounting of the coated lens in the gas stream. The vapochromic compound was drop coated on the optical window after suspension in ether. The SSM was placed in a ½" Swagelok cross with the gas stream running perpendicular to the SSM as to flow over the coated lens.

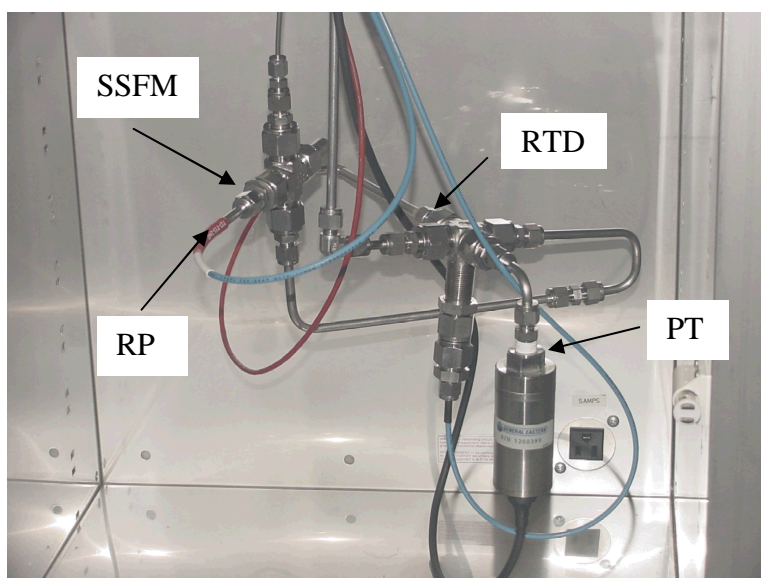


Figure 21 Picture of the sensor probe inside incubator chamber. SSFM – stainless steel flow mount, RP – reflectance probe, PT – pressure transducer, RTD – temperature transducer.

4.2.3 Partial least squares analysis

Luminescence spectra acquired for $[\text{Pt}(\text{phen})(\text{CN-cyclododecyl})_4][\text{Pt}(\text{CN})_4]$ exposed to known levels of ammonia vapor were examined by partial least squares (PLS) analysis. PLS is a multivariate calibration routine that converts the original variables (luminescence intensities and ammonia concentration) into a

non-diagonal covariance matrix. Diagonalizing the covariance matrix produces a new matrix (U) of linear combinations called factors or principle components (PCs). Multiple linear regression of U versus ammonia concentration produces a regression vector that allows the original luminescence intensities to predict ammonia concentration. All luminescence data were normalized and mean centered before PLS analysis was performed using MATLAB. At least three replicate spectra were collected at each ammonia concentration level and used in the PLS model. In each case, a three PC model was sufficient to describe 97% or greater of the variance in the data. The quality of the PLS model fits was estimated by standard R^2 values calculated for each linear regression.

4.3 Results

Initial screening of eleven vapoluminescent compounds was performed in order to determine the optimum material for detecting vapor phase ammonia in the presence of water. Table 7 lists the compounds and the corresponding luminescence properties of each in dry N_2 , ammonia and N_2 and moisture. Since this was only a qualitative test, scores were given to rate the material's response to ammonia and moisture in reference to dry N_2 with 1 being a large response and 4 being no response. Compound 10 (COM10), $[Pt(phen)(CN-cyclododecyl)_4][Pt(CN)_4]$, showed the greatest change in luminescence properties for ammonia while not overlapping with luminescence due to moisture. In addition, Compound 11 (COM11), $[Pt(CN-cyclododecyl)_4][Pt(CN)_4]$, showed the greatest response to moisture and has been demonstrated to be useful as a moisture sensitive vapoluminescence material in a previous study²⁶.

Table 7 Qualitative luminescence properties of screened vapochromic compounds. Ratings: 1 = good, 2 = useable, 3 = minimal response and 4 = no response.

| # | Vapoluminescence Compound | Dry N_2 | H_2O | NH_3 | Ratings | |
|----|---|-----------|--------|--------|---------|--------|
| | | | | | NH_3 | H_2O |
| 1 | $[Pt(CN-n-C_{14}H_{29})_4][Pt(CN)_4]$ | 540 | 545 | 555 | 2 | 2 |
| 2 | $[Pt(CN-cyclohexyl)_4][Pt(CN)_4]$ | 600 | 590 | 595 | 3 | 3 |
| 3 | $[Pt(CN-cyclohexyl)_4][Pt(NO_2)_4]$ | 560 | 560 | 560 | 4 | 4 |
| 4 | $[Pt(phen)(CN-CH_2C_6H_5)_4][Pt(CN)_4]$ | 665 | 630 | 650 | 2 | 2 |
| 5 | $[Pt(CN-CH_3)_4][Pt(CN)_4]$ | 590 | 580 | 560 | 2 | 3 |
| 6 | $[Pt(CN-4-C_6H_4-cyclohexyl)_4][Pd(CN)_4]$ | 660 | - | 561 | 1 | - |
| 7 | $Pt(CN-4-C_6H_4-ethyl)_2(CN)_2$ (purple form) | 755 | 732 | 740 | 2 | 2 |
| 8 | $[Pt(phen)(CN-cyclododecyl)_4][Pt(CN)_4]$ (mixed) | 749 | 735 | 747 | 3 | 1 |
| 9 | $[Pt(phen)(CN-cyclohexyl)_4][Pt(CN)_4]$ (mixed) | 685 | 675 | 705 | 1 | 2 |
| 10 | $[Pt(phen)(CN-cyclododecyl)_4][Pt(CN)_4]$ | 675 | 635 | 705 | 1 | 2 |
| 11 | $[Pt(CN-cyclododecyl)_4][Pt(CN)_4]$ | 745 | 640 | 745 | 4 | 1 |

Luminescence spectra of COM10 were obtained in the presence of known levels of ammonia at constant temperature (25 ± 2 °C). Examples of individual luminescence spectra are shown in Figure 22. In general, the compound quickly and reproducibly responded to changes in ammonia concentration with equilibration times less than 10 s. Recovery times were approximately 10 s also when purged with pure nitrogen. Repeated cycles at 0.05% ammonia showed some hysteresis effects which could be reduced or eliminated by heating the vapoluminescence material during recovery[27]. As shown in Fig. 22, the intensity of the luminescence spectra very slightly shifted to the red as the ammonia concentration

increased from 0.3 to 2.4%. Then between 2.4 and 3.0% ammonia, the spectrum was strictly dominated by an intensity change.

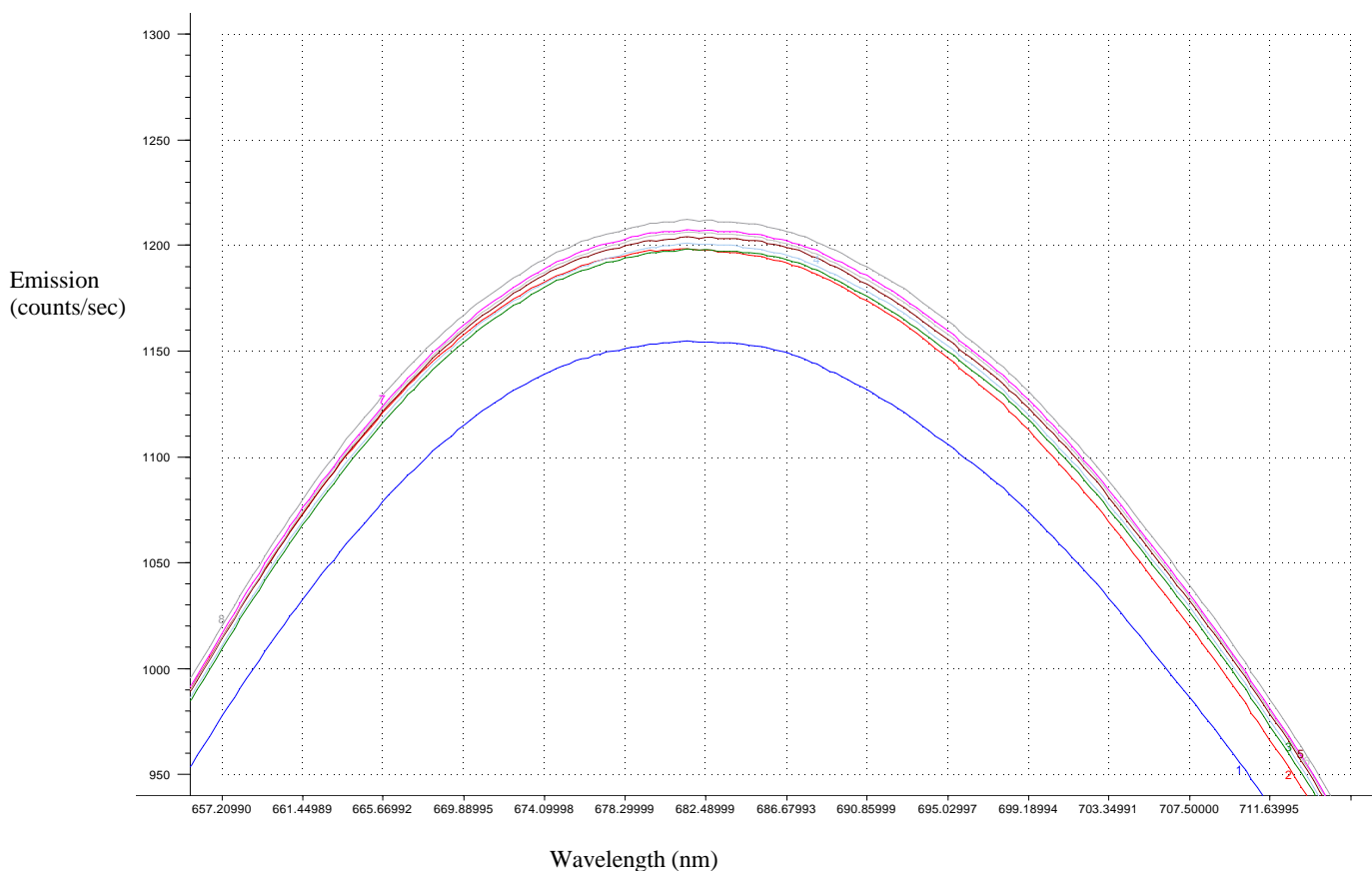


Figure 22 Luminescence spectra of [Pt(phen)(CN-cyclododecyl)₄][Pt(CN)₄] after exposure to increasing ammonia concentration.

Previous work using vapochromic compounds to sense relative humidity have demonstrated that these effects can be utilized to form the transducer mechanism of a luminescence-based sensor[25,26].

To determine the feasibility of COM10 as a linear, quantitatively useful ammonia sensor, the luminescence spectra were examined by PLS. In general, PLS is able to fully utilize the mixture of intensity and wavelength maximum shifts that are found in the luminescence for the vapochromic compound shown in Figure 22. In Figures 23,24, the PLS models for two ammonia concentration ranges (0.3 – 3.0% and 0.7 – 3.0%) are shown. In each case, three principle components are used to describe the variance in the data. Both models gave very linear responses with R^2 values of 0.9733 and 0.9998, respectively. For the 0.3 – 3.0% calibration model (Figure 23), the variance was described by three PCs in the loadings plot (Figure 25). The first PC accounted for the variance due to the intensity change at the higher ammonia levels (> 2.4%) and the second PC accounted for the slight bathochromic (red) wavelength shift over the lower concentrations (< 2.4%). The third PC described a residual shifting at the lower concentration range that was thought to be due to an error in gas mixing or control at the 0.3% ammonia level. By eliminating the 0.3% data point and remodeling over the 0.7 – 3.0% range (Figure 24), a higher linear correlation value was obtained and the variance due to the third PC disappeared.

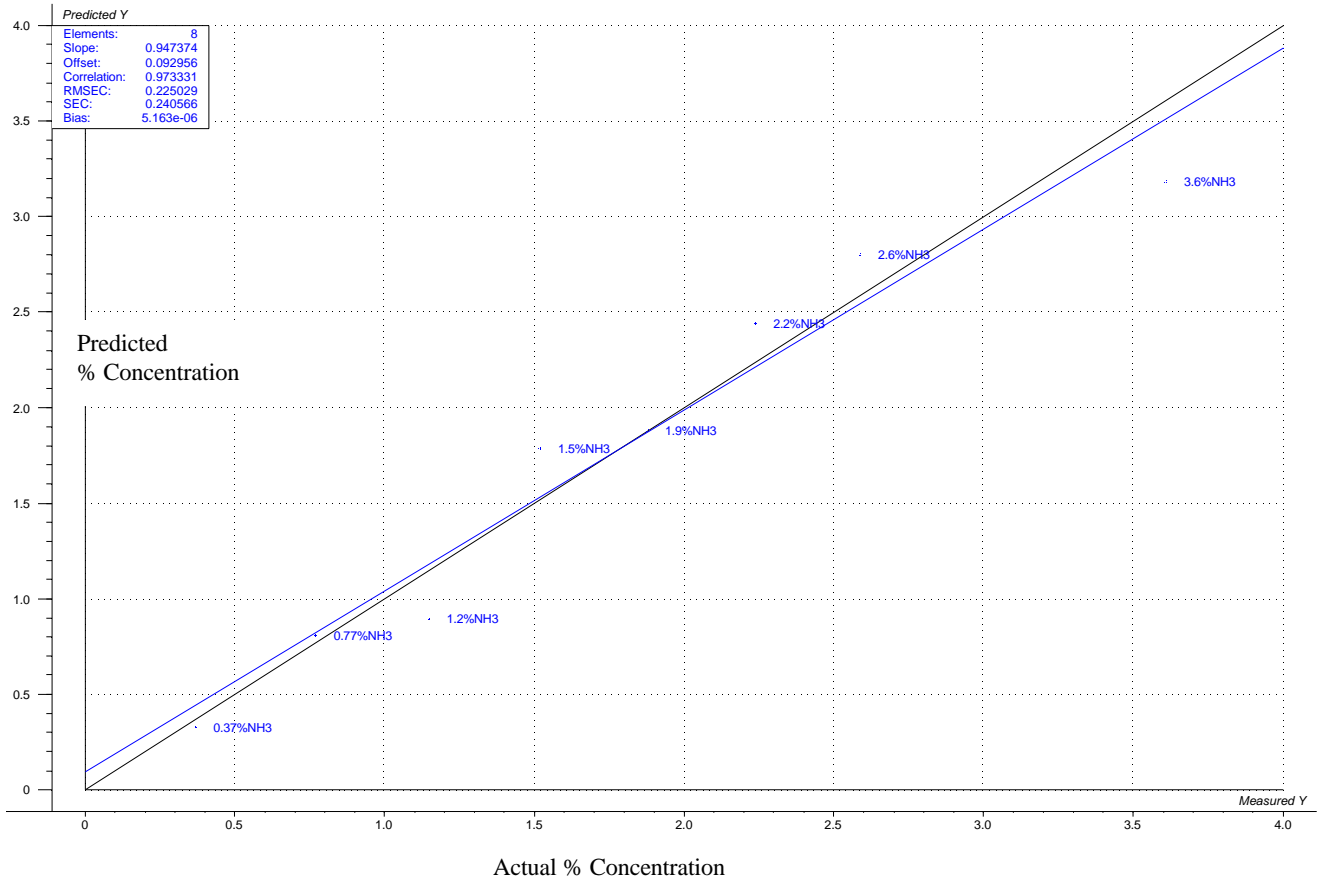


Figure 23 PLS calibration model over 0.3 to 3.0% ammonia. The model captures 97% of the variance in the data.

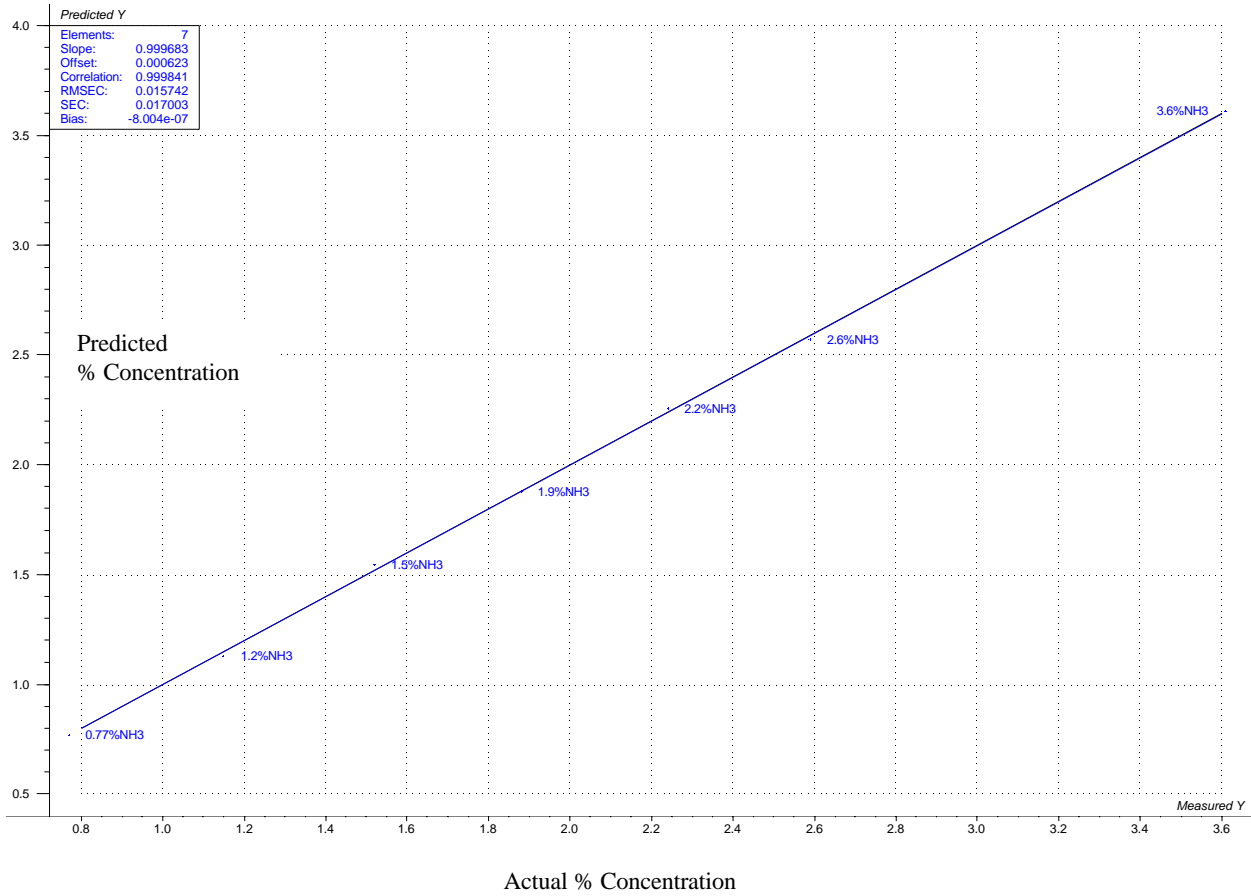


Figure 24 PLS calibration model over 0.7 to 3.0% ammonia. The model captures over 99% of the variance in the data.

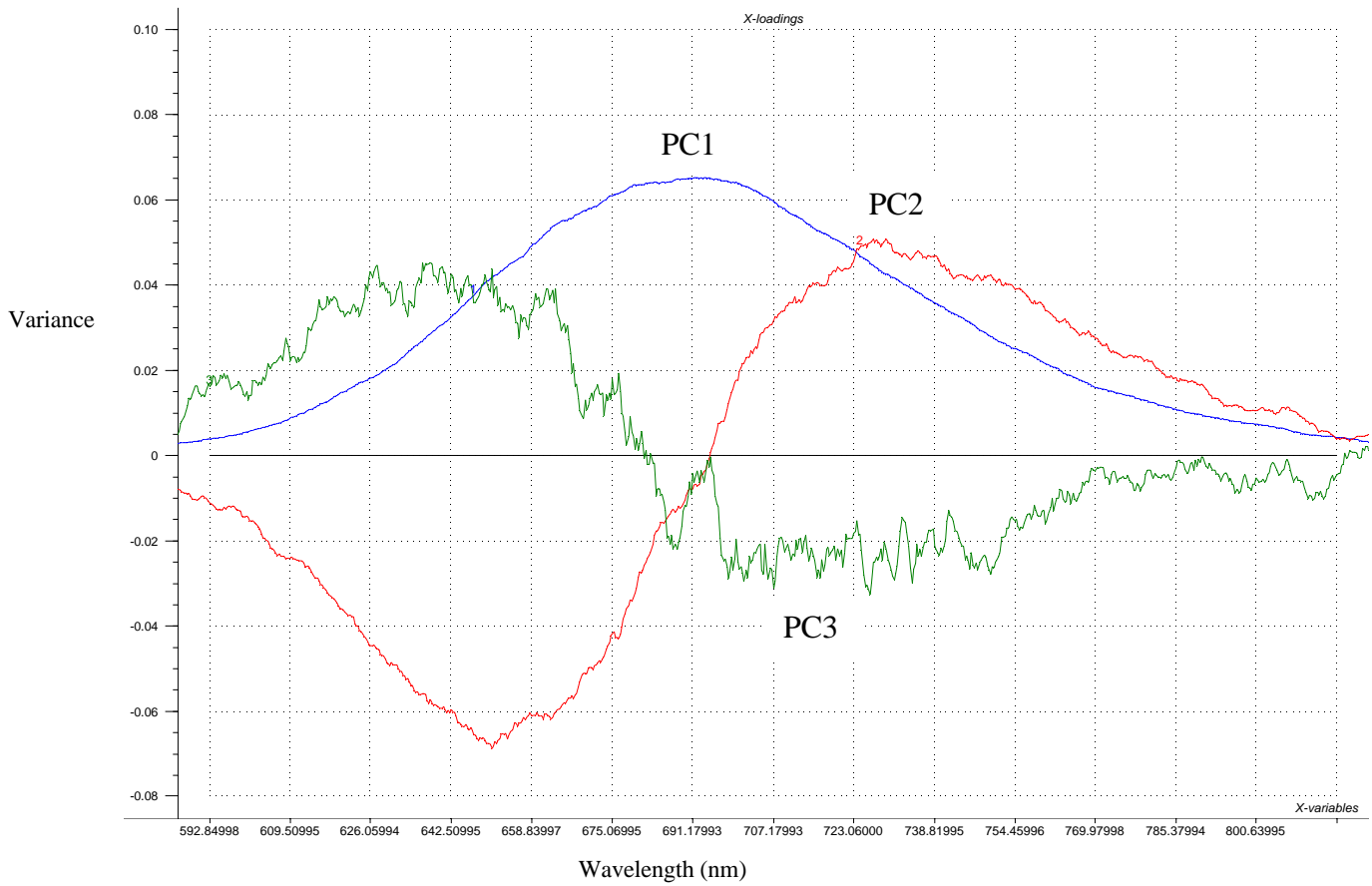


Figure 25 PLS loadings plot over the 0.3 to 3.0% ammonia calibration range. PC1 describes the variance associated with the increase in intensity, PC2 describes the variance due to the bathochromic shift with change concentration and PC3 describes the variance due to residual wavelength shifting at the lower concentration ranges.

4.4 Conclusions

We have demonstrated that vapoluminescence from platinum(II) double salts is a viable mechanism for the measurement of vapor phase ammonia. Initial screening of eleven vapoluminescence compounds indicated that at least one, $[\text{Pt}(\text{phen})(\text{CN-cyclododecyl})_4][\text{Pt}(\text{CN})_4]$, showed promise to detect ammonia in the presence of moisture. PLS modeling of that compound demonstrated a linear response ($R^2 = 0.9998$) from 0.7 to 3.0% ammonia concentration with a sensitivity of at least 0.2% which was limited by the control of the gas manifold. In general, the compound quickly and reproducibly responded to changes in ammonia concentration with equilibration times less than 10 s. Recovery times were approximately 10 s also when purged with pure nitrogen. The vapochromic compound did show some effects of hysteresis while it is thought that this can be overcome by simple heating of the material during the recovery cycle.

4.5 Recommendations/Path Forward

It is the opinion of the authors that these vapochromic compounds would make viable percent level (>0.5%) ammonia sensors, but do not meet the needs for the Tritium Facilities at the low to sub-ppm (0.00001%) level ammonia concentration.

5.0 MINIATURE INFRARED SENSORS

5.1 Introduction and Background

The Palladium Membrane Reactor (PMR) is designed to recover hydrogen isotopes from water present as an impurity in tritium processing activities.[31,32,33] In the PMR, water and carbon monoxide (CO) are catalytically reacted to form carbon dioxide (CO₂) and hydrogen at elevated temperatures and pressures (up to 425 °C and 2-3 atmospheres, respectively). The hydrogen is recovered by diffusion through a palladium (Pd) membrane (driven by the partial pressure difference between the process pressure on one side and vacuum on the other side), which is selectively permeable to hydrogen. Most hydrogen will be present as protium. Only trace amounts of deuterium and tritium are expected.

The efficiency of the PMR reaction is governed by the CO/water concentration ratio. A slight excess of CO improves the kinetics of the reaction and promotes complete conversion of the water to elemental hydrogen; however, too much CO leads to fouling of the catalyst and/or Pd membrane with elemental carbon (soot), degrading the performance of the PMR. The recent failure of several Pd membrane tubes at the SRNL may be attributable in part to an excess of carbon, which may have been incorporated into the metallic structure, making it more susceptible to deformation and leaking.

The desired CO/water ratio is within a narrow range, 1.05-1.1. This suggests that the water and CO pressures must each be measured with absolute accuracies of 1-1.5% to obtain effective process control.¹ The consequences of operation outside this band for an extended period of time highlight the need for accurate quantitation and control of the feed gases. The historical approach used to maintain the proper ratio is to measure and control the mass flow rates of each species individually before mixing them. Development work at Los Alamos National Laboratory (LANL) and SRNL has shown this approach to be not entirely satisfactory, as the mass flow measurement devices have not been sufficiently accurate to prevent process upsets. Therefore, flow control based on a more precise and reliable measurement technique is desirable.

Several techniques which have been widely applied to the general problem of process gas analysis include gas chromatography (GC), mass spectroscopy (MS), and infrared spectroscopy (IR).[34] However, GC and MS are not particularly suitable to PMR feed gas analysis. The feed gas is maintained at temperatures near 140 °C to keep water vaporized at high pressures. Process measurements with both GC and MS require capillaries to transport the sample to the instrument. Thus, extensive heat tracing is required to keep water from condensing in the lines, and the finite transport time of the gas makes these methods less responsive. Also, procurement and maintenance costs for these instruments are substantial.

Infrared spectroscopy is more amenable to the analysis problem, as it is readily introduced into the process environment and the target analytes are detectable at the process conditions. There are several IR techniques which could be considered. Fourier transform absorbance [35] and

¹ For example, a 1.25% uncertainty for a target CO pressure of 1.075 atm yields a range of 1.062 – 1.088 atm. To maintain the CO/water ratio within the desired limits, the H₂O pressure must be between 0.989-1.011 atm. This range represents a 1.1% spread from the target pressure of 1.0 atm.

emission [36] spectroscopy, tunable diode laser spectroscopy [37], and cavity ring-down (time-based) spectroscopy [38] have all been successfully demonstrated for trace gases, and are commercially available. However, the capabilities of these methods are all far greater than what is required for the application. Instead, we have concentrated on finding a simple instrument that can be economically installed at several locations and is easy to operate.

Infrared plug sensors [39] meet this description. The plugs are small, rugged, and self-contained². They can be placed directly in the process stream and do not require fiber optics. They can be obtained in a variety of sampling configurations. Liquids and solids can be measured with attenuated total reflection on a single plug, while gases are analyzed by absorbance across the pipe diameter with separate source and detector plugs. Since the water and CO are the only stream constituents, and have absorptions that are spectrally distinct, an IR spectrometer is not required for the measurement. Instead, one may simply use two or three detectors whose wavelength responses are defined by bandpass filters.

This report describes characterization work done on one type of sensor, the Infraran model produced by Wilks Enterprises (Norwalk, CT). We studied the temperature and pressure dependence of the sensor response, potential interference effects occurring from different gas mixtures, short- and long-term accuracy and precision, the effect of different signal averaging options, and other environmental effects.

5.2 Experimental

5.2.1 Sensors

Figure 26 shows the gas cell and the sensor housing. The light source (labeled “A”) is a pulsed diamond thin-film element, with an output approximated by a black body temperature of 800-850 °C. There are two pyroelectric detectors mounted in a T08 can housing on the opposite side of the cell from the light source (labeled “B”). Glued in front of each detector is an infrared bandpass filter corresponding to either CO or H₂O vibrational absorptions (near 4.7 and 2.7 μm, respectively). Figure 27 shows the blackbody emission and filter transmission spectra for these elements. No reference detector was provided. The source and detector interface the gas cell through cubic zirconia windows (2 mm thickness, 12.5 mm diameter) which are sealed with epoxy. The windows define a 3 mm absorption path length.

² Typically the plugs are 2” diameter. They have been tested to 150 psi and 100 °C. The light source and detector are mounted on the plug. Processing electronics can be on the plug or in a separate box.

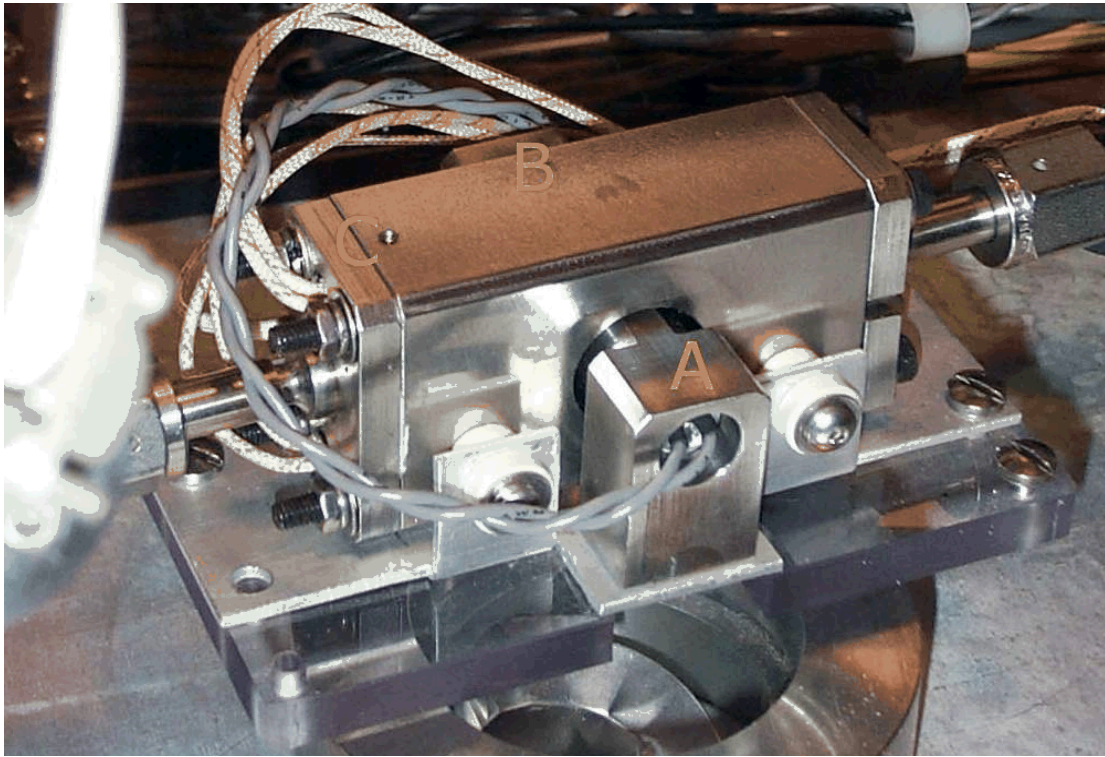


Figure 26 Photograph of infrared cell.

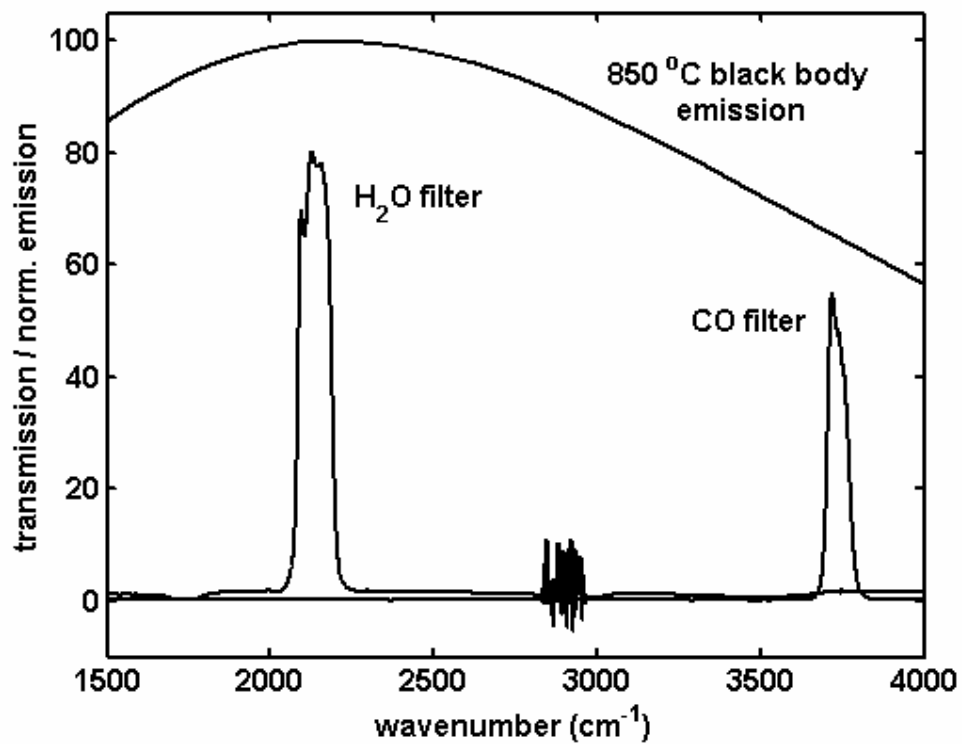


Figure 27 Spectral profiles of IR filters and source.

The sample cell is constructed from stainless steel and is approximately 10 cm long and 2.5 cm wide. The internal cell volume has a rectangular cross-section 3 mm wide and 10 mm high. End caps with ¼" female VCR fittings are attached to the cell with four pass-through bolts; seals are maintained with rubber gaskets. There are three holes in the sample cell body parallel to the internal cell. Two holes house cartridge heaters (labeled "C" in Figure 26), and the third contains a thermocouple. These elements are connected to a temperature regulator.

Other supporting electronics include a control module that provides power to the source and detectors and monitors the detector output, and a processing unit that maintains the calibration and displays results. Output can also be logged onto a computer through a standard serial cable connection.

5.2.2 Gas Handling

The sample cell was spliced into a gas handling manifold which had previously been constructed for testing a PMR prototype. All lines were heat-traced by wrapping them in heating tape, foam insulation, and aluminum foil, and installing thermocouples to monitor the temperature. Minimum temperatures of 120 °C were set in order to maintain water in the vapor phase at elevated pressures. Pressure was measured at several points in the manifold, including adjacent to the gas cell. CO was introduced from a standard gas cylinder (Scott). Steam was taken from a facility steam line. The entire gas system, including the sensor but not the display electronics, was contained in a large walk-in hood. Several CO and CO₂ atmospheric sensors were employed to monitor leaks.

Sensor readings were obtained with gas pressures ranging from 14.5 - 40 psi. Readings were made on a static system. The pressure was varied by sequentially bleeding in or releasing a small amount of gas and allowing the system to equilibrate for 30-60 seconds. This time period was determined both by the signal averaging of the instrument (typically 30 seconds) and by gas transport issues associated with the narrow dimensions of the cell.

In the course of the work, two problems developed which precluded us from making all the desired measurements. First, it proved to be very difficult to maintain heat tracing so that water vapor did not condense somewhere in the line. Thus, water measurements were made on a dynamic system, where the instantaneously measured absorbances were compared with instantaneous pressures. Thus, the data obtained for those experiments did not have the same advantage of signal averaging as the CO data. Second, we intended to create CO/H₂O mixtures inside the sample cell by introducing a known pressure of one gas into the cell and then applying a greater pressure of the second gas. In testing this arrangement with CO and argon, we found that we could not remove residual amounts of the first gas added from lines leading to the cell. Thus, when the second gas was added, it swept in a certain amount of the first gas, and thus partial pressure of the first gas was not left constant. Due to time and equipment constraints, we were not able to install a vacuum pump to clear out those lines. We also could not heat trace a reservoir which would have been a more suitable gas mixing chamber.

5.2.3 Calculations

Sensor response calculations were performed with Matlab, version 6.1 (Mathworks, Natick, MA). IR absorption spectra of CO and H₂O were calculated from the 2000 HITRAN database using HITRAN-PC (ONTAR, N. Andover, MA). Bandpass filter spectra were provided by the vendor. Light source output was calculated assuming an 850°C black body source with a Web-based applet from Lawrence Berkeley Laboratory [40].

5.3 Results and Discussion

5.3.1 Experimental Results

The sensor testing concentrated on those aspects associated with use in a process environment. Process temperature and pressure variations, external influences, and chemical changes must all be accommodated. A sensor could be insensitive to these factors, or its variations must be corrected by incorporating other measurements (typically pressure and temperature). Stability of the sensor, independent of process changes, must also be considered. A thorough understanding of these factors is required to assess both the viability of the sensor for the application and the resources needed to install and operate the sensor.

5.3.2 Sensor Stability

The Infraran sensors are designed to be operated at temperatures below 80-100 °C. The limiting factor is expected to be the temperatures at which the on-board electronics can reliably operate. Since the gas temperature in the PMR system must be 120-140 °C to keep water in the vapor phase and improve the system efficiency, some accommodation must be made to protect the sensors while making the measurement. For the current system, this is done by using ceramic standoffs to maintain physical separation of the sensor mounting brackets and the gas cell. However, the separation between the sensor and the cell is only a few millimeters, and thus the sensors are likely to be near the upper end of their recommended operating temperature.

We therefore conducted a stability test to show that the sensors would operate effectively under these conditions. The cell was heated to 120 °C, pressurized with Ar (~39 psi), and sealed. The sensors were zeroed and the system was maintained at these conditions for over 30 hours. The measured absorbances (using a 30-second rolling average) for both CO and H₂O channels are shown in Figure 28. With the exception of a relatively large spike near 1000 minutes, as seen in Figure 28a, and a similar feature at the beginning of the study, the response of both sensors is stable (standard deviations of 0.0032 and 0.0046 absorbance units (au), respectively).

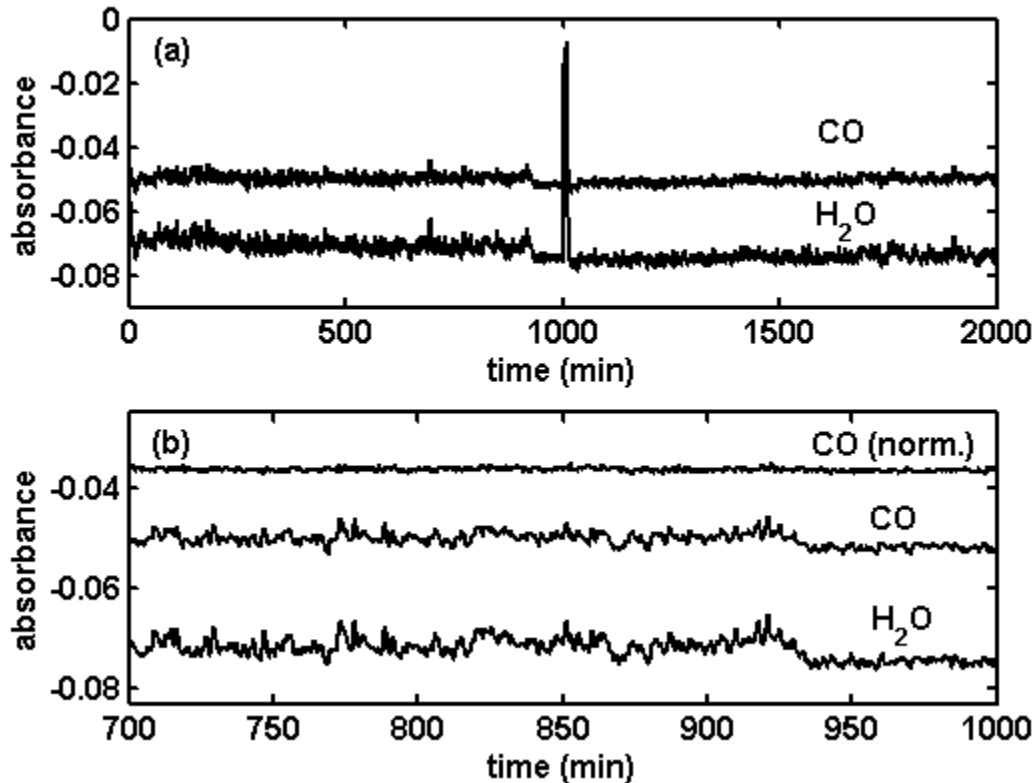


Figure 28 Stability and noise characteristics of detectors.

Several features of the figure merit further discussion. The sensors were located inside a walk-in vent room. After the sensors were zeroed, the vent room doors were closed, and both sensors recorded a 0.05-0.07 au offset that was maintained as long as the doors were closed. The sharp spikes back toward zero occurred when the doors were opened to look at the sensors. Further investigation revealed that when the doors were closed, there was a strong air flow through an opening at the top of the room directly onto the sensors, presumably cooling them. This behavior suggests that if the Infran were to be used in a hot process environment, care would have to be taken to have the environmental conditions remain as consistent as possible. Sensor drift on this scale is much greater than the intrinsic sensor noise, and is significant on the scale of absorbance changes caused by CO and H₂O with this gas cell.

An expanded view of the sensor response (Figure 28b) shows that the CO and H₂O noise is highly correlated ($\rho = 0.79$), supporting the suggestion that environmental variations in this test are greater than intrinsic sensor variations. The latter can be estimated by treating the H₂O channel as a reference and dividing it into the CO channel response to normalize the latter. After multiplying by the H₂O channel average (about 0.07 au), one obtains the top trace in Figure 28b, which has less variation than the individual curves. The standard deviation of the normalized set is 0.00091 au, which is 3.5 times better than the raw signal. The improved performance strongly suggests that a reference channel should be used in future configurations.

5.3.3 CO Sensor

Absorbance values as a function of system pressure were obtained for 100% CO at temperatures ranging from 23 - 140 °C. The absorbance increased monotonically with pressure increase, and the results are reproducible across several pressure cycles. Typical data (120 °C) showing the dependence of pressure (measured in absolute psi) on absorbance, along with a best fit line, are shown in Figure 29. Although the absorbance was the dependent variable during data collection, it is shown as the independent variable to be more representative of how the sensor would be used in practice.

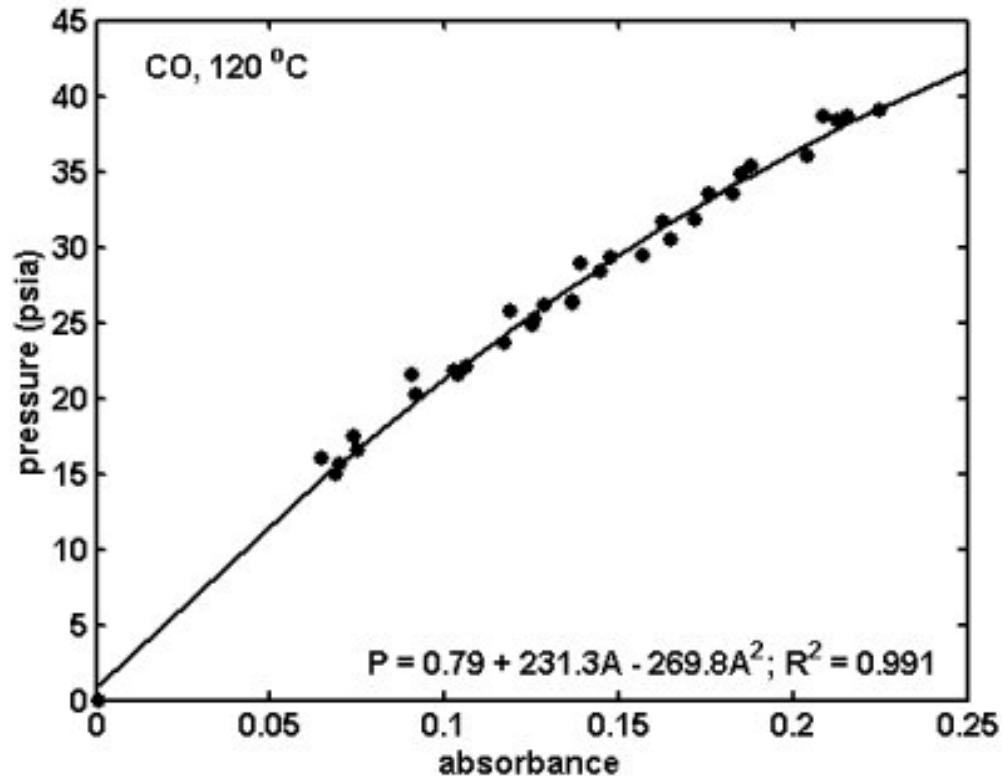


Figure 29 Relationship between pressure and absorbance for CO.

Table 8 shows the quadratic fit parameters for each temperature ($P(\text{psia}) = a_0 + a_1A + a_2A^2$). Several points are apparent. The intercepts (a_0) are zero or nearly zero for all temperatures. The linear coefficients (a_1) generally increase with temperature. This may be expected if the increasing temperatures result in the population of higher rotational levels, which would lead to more absorption lines appearing within the filter bandpass (at the expense of lines outside the bandpass). Thermal expansion of the cell may also account for a small portion of the increase. The quadratic term (a_2) is statistically significant at all temperatures, which represents a deviation from the linear behavior predicted from Beer's Law.³ However, nonlinearity may be expected under certain conditions which are met in these measurements. This topic will be further examined during the discussion of sensor response calculations, below.

³ $A = \epsilon bc$, where ϵ is the absorptivity of the molecular transition, b is the measurement pathlength, and c is the concentration.

Table 8 Temperature dependence of CO absorbance.

| T (°C) | a ₀ (1σ) | a ₁ (1σ) | a ₂ (1σ) | R ² | Std err (%) |
|--------|---------------------|---------------------|---------------------|----------------|-------------|
| 23 | 0.88 (0.76) | 129 (7) | -49 (17) | 0.9976 | 1.6 |
| 50 | 0.03 (0.55) | 160 (6) | -105 (18) | 0.9894 | 2.6 |
| 85 | 2.3 (0.7) | 188 (10) | -154 (34) | 0.979 | 3.3 |
| 120 | 0.8 (0.7) | 231 (11) | -270 (42) | 0.991 | 3.3 |
| 140 | 4.7 (0.3) | 220 (5) | -181 (22) | 0.9982 | 1.4 |

Note also that each fit replicates the measurements within 2-3%. This accuracy is consistent with the control requirements described above. However, these tests were conducted under controlled conditions and were of a relatively short duration. Greater uncertainties, and the need for compensatory measurements, would be expected in less controlled conditions.

5.3.4 H₂O Sensor

For reasons described in the experimental section, it was not possible to get time averaged absorbance data for a fixed water vapor pressure in the cell. Consequently, the uncertainties associated with this analysis are greater than for the CO analysis. There is no reason otherwise that the analysis of water vapor should be any less accurate than for CO; therefore, the results reported here should not be considered a true measure of the potential system performance. Data was only acquired at 140 °C, so no temperature dependence of the coefficients was obtained. The 140 °C data is presented in Figure 30. The sensor response to water is similar to the CO response, particularly with the statistically significant negative quadratic dependence on absorbance.

5.3.5 Analyte Independence

Because both the water and CO measurements are univariate (relying on the signal of a single detector), accurate measurement of each requires that the measurements be independent. Independence must not only be intrinsic, e.g. there are no overlapping absorption peaks, but also extrinsic, e.g. water and CO do not interact so as to appreciably change the absorption of either.

Intrinsic independence is expected based on calculations using the HITRAN atmospheric database; there are no CO absorptions predicted in the 3680-3800 cm⁻¹ range of the H₂O filter, nor are there H₂O absorptions in the 2060-2210 cm⁻¹ range of the CO filter. Measurements of pure CO and pure H₂O vapor confirm this result. The correlation coefficient (ρ) for the CO sensor in the presence of water is 0.12. The correlation coefficient for H₂O in the presence of CO is somewhat larger, 0.29, but this value may reflect environmental effects, as discussed above. These results confirm that the detectors are intrinsically independent.

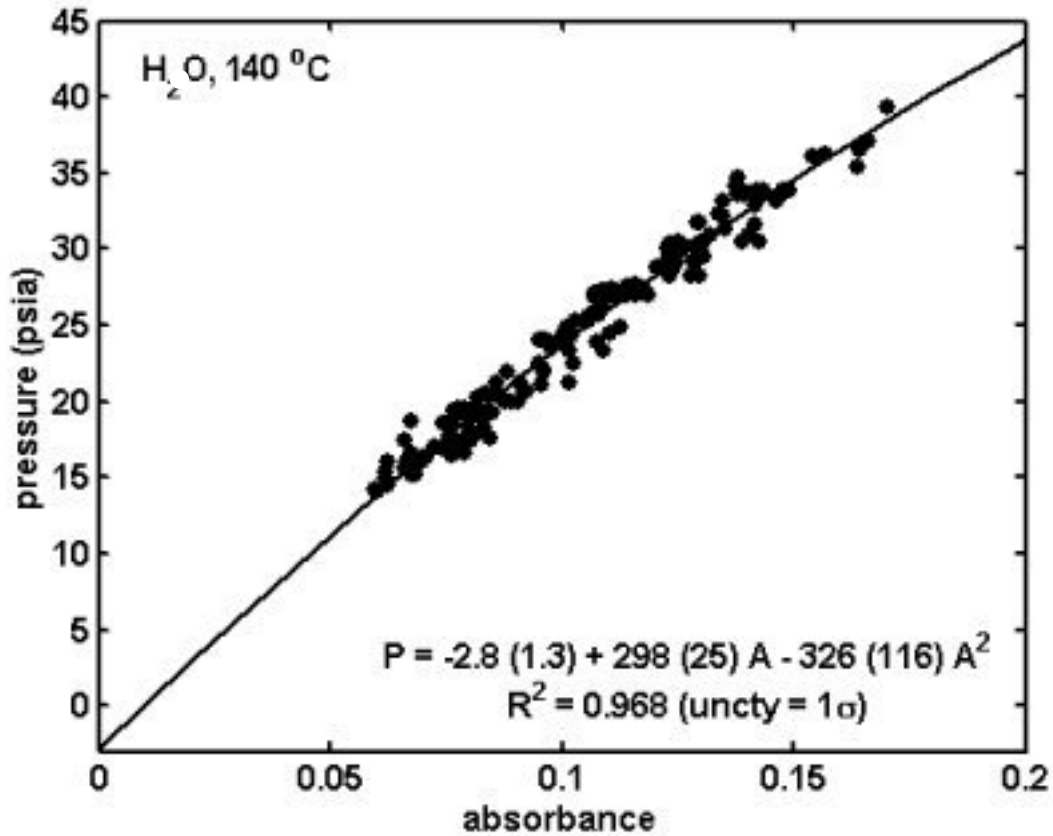


Figure 30 Relationship between pressure and absorbance for H₂O.

Extrinsic interactions may be considerable given the strong hydrogen-bonding potential of H₂O and CO. The effect of these interactions on gas number density, which in turn affects absorption, can be estimated from the van der Waals gas equation [41]:

$$\left(P + \frac{a}{v^2}\right)(v - b) = RT$$

$$v = \frac{V}{n}$$

Here, P, V, and T are the system pressure, volume, and temperature, R is the ideal gas constant, n is the total moles of gas, and a and b are molecule-specific interaction constants. The molar gas density is represented by v^{-1} . For a mixture, the effective interaction constants can be determined from the constants for the components:

$$a_{\text{eff}} = \sum_i \sum_j f_i f_j (a_i a_j)^{1/2}$$

$$b_{\text{eff}} = \sum_i \sum_j f_i f_j (b_i b_j)^{1/2}$$

where each summation is over all components, and f_i is the molar fraction of the i^{th} component.

The effect of water on CO number density, and *vice versa*, can be seen in Figure 31. Here, the partial pressure of the labeled component is fixed at 14.7 psia (1 atm), while the partial pressure of the other component varies from 7.35 to 22.35 psia. The effect is plotted as a deviation from the ideal gas law. This calculation also takes into account self-interactions (e.g. CO-CO or H₂O- H₂O). It may be seen that near the typical PMR operating conditions of 2 atm total pressure, the number density correction for each gas is approximately 0.5%. The correction changes by a few tenths of a percent with expected temperature and pressure variations within the PMR process.

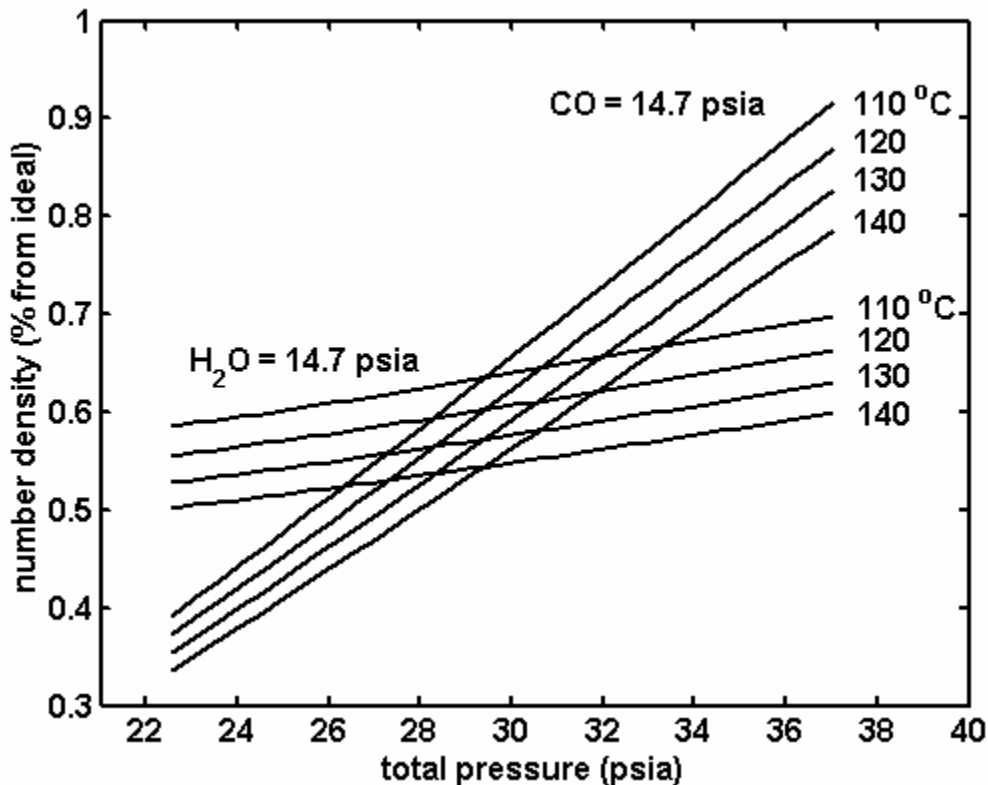


Figure 31 Pressure-dependent deviation from ideal gas law.

This change is significant compared to the desired 1-1.5% uncertainty of the measurement. However, a correction based on a temperature measurement can be made readily. As both intrinsic and extrinsic interactions are negligible or correctible, we can conclude that the water and CO signals are adequately independent.

5.3.6 Signal Averaging

The sensor manufacturer supplied the control system with a fixed rolling average of 30 seconds applied to the displayed gas concentrations. We wished to determine if a shorter time constant would provide adequate noise reduction while allowing for a faster system response. The data stream includes instantaneous intensity readings, which can be converted to absorbances. A section of this data for a CO

cycling experiment is shown in Figure 32. In addition to the raw data, data averaged over 7.5, 15, and 30 seconds is shown. Averaged data is offset for clarity.

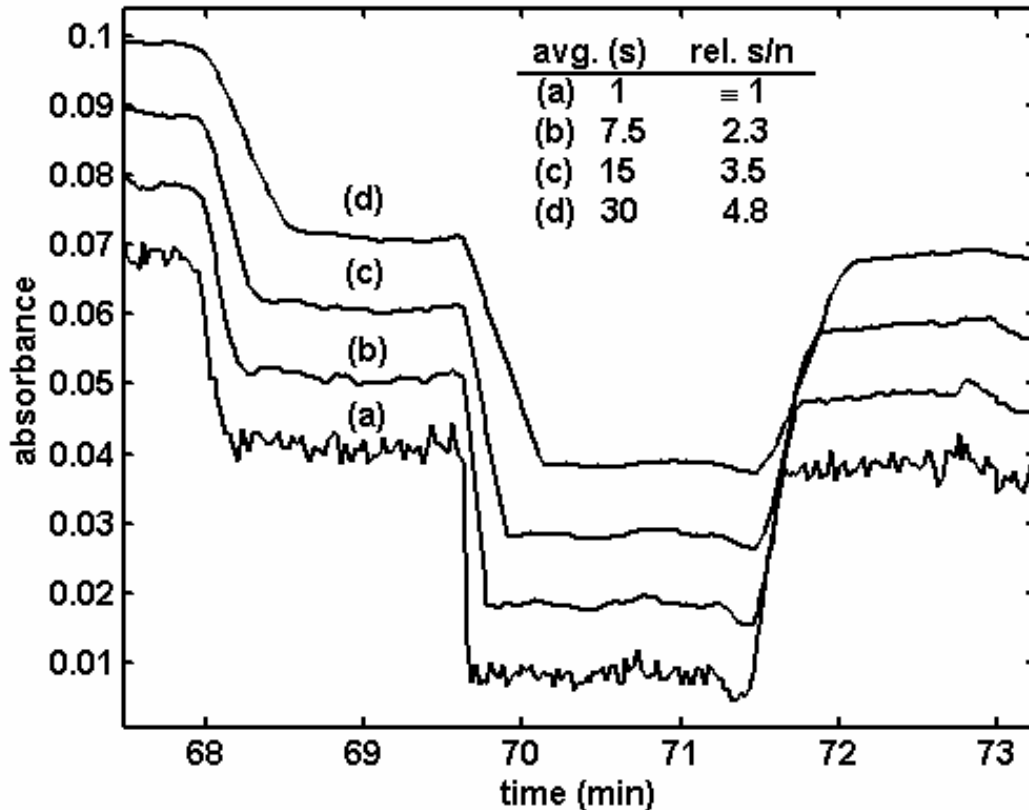


Figure 32 Effect of signal averaging.

Noise reduction, as measured by the standard deviation of the signal with constant CO, improves at a rate slightly less than the square root of the relative time constant. The effect of the time constant on the response to a (near-)instantaneous change in gas concentration can also be seen.

The fit results of Table 8 suggest that the longer signal averaging should be maintained. However, as environmental variations have been shown to play an important role in sensor response, the use of a dedicated reference detector may allow for a shorter averaging time.

5.4 Calculation Results

We supplemented the experimental measurements with calculations simulating sensor response under a variety of conditions. In some cases, this approach was required because we could not successfully prepare gas mixtures with water vapor. In other cases, the sensor/flow cell configuration (e.g. pathlength) could not be changed. The calculations expand our understanding of sensor properties. They can also serve as a template for predicting the viability of the sensors for applications with different operating conditions and/or analytes.

5.4.1 Methodology

The signal generated by each detector can be calculated by convolving the effects of each optical element on the spectrum of the light propagated through the system. The four primary elements are the source, sample, filters, and detector:

$$S(\omega) = I_{\text{lamp}}(\omega) \times T_{\text{sample}}(\omega) \times T_{\text{filter}}(\omega) \times Q_{\text{detector}}(\omega),$$

where S represents detector signal, I light intensity, T transmission, and Q quantum efficiency, all of which are dependent on the light frequency, ω .

Several assumptions are made with the calculations. Detector efficiency is assumed constant over the frequency range defined by an individual filter ($Q_{\text{detector}} = 1$). Likewise, any reflections at the interfaces in the optical path are assumed not to have a frequency dependence.

Calculations are made for a discrete array of frequencies defined by the highest-resolution data set, which in this case is T_{sample} . The other factors, I_{lamp} and T_{filter} , are interpolated to the higher resolution with a spline fit. Calculations were made with different resolutions for T_{sample} , and consistent results were obtained for resolutions smaller than or equal to 0.01 cm^{-1} . Because the finer resolutions require a larger data set, the maximum spacing was used for subsequent calculations.

S is summed over all frequencies to determine a total signal. Absorbance is calculated from the ratio of the signals for a “zero” gas and the analyte:

$$A = -\log_{10} (S_{\text{analyte}} / S_{\text{zero}}).$$

T_{sample} is calculated using the HITRAN database [42], which includes linewidth, intensity, pressure coefficients, and other parameters for all observed infrared, visible, and ultraviolet spectral lines for a number of atmospherically important small molecules. The calculation of gas transmission profiles requires the control of a large number of parameters. All gas concentrations apart from H_2O and CO were set to zero. Temperatures and partial and total pressures were specified. A horizontal beam path was selected to remove any altitude effects on the calculation. The smallest available pathlength (1 cm) was chosen. As this value is larger than the gas cell pathlength (0.3 cm), a correction to the results was made (see below).

5.4.2 Comparison to Experiment

The ability of a calculation to replicate experimental results gives a measure of confidence for subsequent calculations. There are two experiments in this study for which a comparison can be made – measurement of CO absorbances at a given temperature, and the replication of temperature-dependent absorption trends for CO .

The comparisons require a correction of the long pathlength used in the calculations. Beer’s Law, which describes a linear relationship between pathlength and absorbance, does not apply when absorbances are saturated (e.g. all of the light at a certain frequency is absorbed by the sample). In these cases, the absorbance will be less than predicted from a linear extrapolation from shorter pathlengths. This is seen in Figure 33, which shows the calculated absorbance for different pathlengths and CO pressures. There is a readily apparent quadratic component to the dependence that is more pronounced for higher pressures. This feature is consistent with more saturated transitions within the filter transmission envelope at the

higher pressures. It is also interesting to note the onset of nonlinearities at relatively low absorbances. This occurs because the absorbance is an integrated quantity that includes both saturated transitions and regions with no absorbance. Therefore, the average absorbance for the region is less than what is normally observed when a transition becomes saturated.

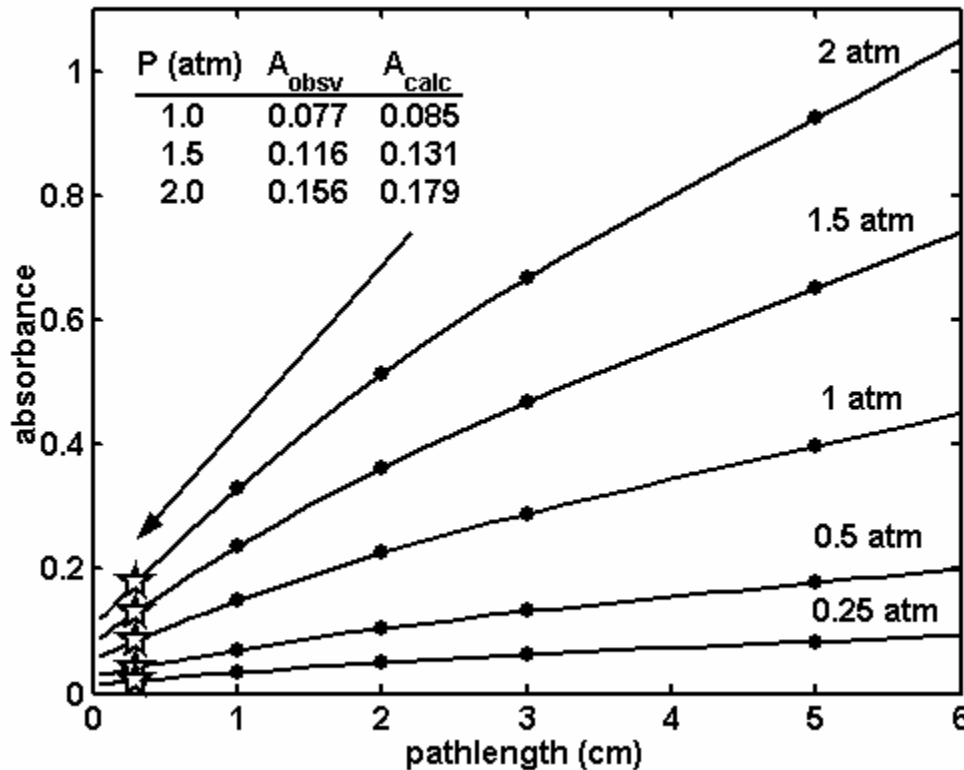


Figure 33 Relationship of pathlength and absorbance.

There are hundreds of narrow absorbance lineshapes within the filter transmission envelope. The number of saturated transitions increases with increasing pathlength, and is non-zero at the shortest available pathlength for the calculation. It is reasonable to assume that at shorter pathlengths, the number of saturated transitions will decrease proportionally. Thus, we can estimate absorbances for the cell pathlength by extrapolating a spline fit to the calculated absorbances. The predicted absorbances for the cell are shown by the stars in Figure 33, and the values are compared to experimental results in the inset. There is good agreement between the two values, considering the inherent assumptions. The agreement indicates that the calculations are representative of experimental results.

A similar level of agreement between experiment and calculation is seen for the temperature dependence of absorbance, as shown in Table 9. Here, the CO or H₂O pressure was fixed at 14.7 psia (1 atm). Absorbances are calculated for 1 cm and corrected to 0.3 cm by dividing by 1.75, the ratio determined from Figure 33.

Table 9 Temperature dependence of CO and H₂O absorbance.

| Temp (K) | 298 | 323 | 358 | 393 | 413 |
|---|--------------|--------------|--------------|--------------|--------------|
| A _{CO} (obsv.) | 0.115 | 0.100 | 0.072 | 0.071 | 0.063 |
| A _{CO} (calc.) | 0.103 | 0.098 | 0.093 | 0.088 | 0.085 |
| A _{H₂O} (calc.) | 0.063 | 0.062 | 0.061 | 0.060 | 0.059 |
| A _{CO} / A _{H₂O} | 1.63 | 1.58 | 1.52 | 1.46 | 1.43 |

The observed and calculated CO absorbances both decrease as temperature increases (the temperature dependence is less marked for the calculation). One contributing factor is the decrease in CO number density caused by fixing both pressure and volume while changing the temperature. Another is a temperature-induced population shift to higher rotational ground states that favors transitions that are outside the filter envelope.

The ability of the calculations to replicate CO absorption measurements and temperature-dependent trends gives a measure of confidence that similar calculations will give good results.

5.4.3 Temperature Effects on Water Absorbances

Table 9 also shows the calculated effect of temperature on water measurements. As with CO, there is a decrease in the absorbance, though the decrease is much smaller (6% versus 17% between 298 and 413K). This is due to the rotational energy level distribution for water. For this symmetric top molecule, transitions from different rotational ground states are interspersed instead of being in a regular progression, as is the case for a diatomic molecule. Thus, population transfer to higher energy states does not change the line overlap with the filter envelope as much as occurs for a diatomic.

Note that the ratio of the CO and H₂O absorbances changes by 2% in the expected PMR process range of 120-140 °C. This deviation can be readily corrected if the temperature is independently measured.

5.4.4 Pressure Broadening

Molecular absorption profiles are sensitive to pressure broadening effects. [43] Specifically, linewidths will increase due to a decrease in excited state lifetimes and an increase in energy level perturbations. This effect is manifested through an intrinsic change in the analyte (the absorptivity) and so differs from the extrinsic changes described above. Note that for a strongly saturated transition, the peak will remain saturated despite the transfer of absorption strength to the wings of the transition. Since there are many such transitions within the filter envelope, pressure broadening is expected to increase the overall absorbance at a given analyte partial pressure.

Pressure broadening effects for CO and H₂O were calculated for expected PMR process conditions. The target gas was assumed to have a partial pressure of 14.7 psia (1 atm), with air providing the balance of

the total pressure.⁴ Total pressure ranged from 26.5 to 32.3 psia (1.8 – 2.2 atm). The temperature was fixed at 140 °C. The pathlength was 0.01 m. Results of the calculation are shown in Table 10.

Table 10 Pressure broadening of CO, H₂O absorbance.

| P _{total} (atm) | 1.8 | 1.9 | 2.0 | 2.1 | 2.2 |
|--|--------------|--------------|--------------|--------------|--------------|
| A _{CO} (0.25 atm) | 0.198 | 0.203 | 0.209 | 0.214 | 0.219 |
| A _{H₂O} (0.25 atm) | 0.126 | 0.128 | 0.130 | 0.132 | 0.134 |

The expected absorbance increases are observed for both CO and H₂O, although the increase is proportionally greater for CO (11%) than H₂O (6%). This may be due to a higher density of saturated transitions within the filter envelope for CO. Different air broadening parameters for CO and H₂O [42] may also have a small effect. The increases are sufficiently large to merit a post-measurement correction to meet PMR control requirements.

5.5 Conclusions and Recommendations

The primary goal of this work is to determine the suitability of the Infraran sensor for use in the Palladium Membrane Reactor. This application presents a challenge for the sensor, since the process temperature exceeds its designed operating range. We have demonstrated that large baseline offsets, comparable to the sensor response to the analyte, are obtained if cool air is blown across the sensor. We have also shown that there is a strong environmental component to the noise. However, the current arrangement does not utilize a reference detector. The strong correlation between the CO and H₂O sensor responses to environmental changes indicate that a reference detector can greatly reduce the environmental sensitivity. In fact, incorporation of a reference detector is essential for the sensor to work in this application.

We have also shown that the two sensor responses are adequately independent. Still, there are several small corrections which must be made to the sensor response to accommodate chemical and physical effects. Interactions between the two analytes will alter the relationship between number density and pressure. Temperature and pressure broadening will alter the relationship between absorbance and number density. The individual effects are small – on the order of a few percent or less – but cumulatively significant. Still, corrections may be made if temperature and total pressure are independently measured and incorporated into a post-analysis routine. Such corrections are easily programmed and automated and do not represent a significant burden for installation.

The measurements and simulations described above indicate that with appropriate corrections, the Infraran sensor can approach the 1-1.5% measurement accuracy required for effective PMR process control.

⁴ HITRAN does not provide any means for distinguishing pressure broadening effects due to different gases, e.g. the broadening of CO from water instead of air. Further literature searching or empirical measurements may be required to determine precisely any required correction.

It is also worth noting that the Infraran may be suitable for other gas sensing applications, especially those that do not need to be made in a high-temperature environment. Any gas with an infrared absorption (methane, ammonia, etc.) may be detected so long as an appropriate bandpass filter can be manufactured. Note that homonuclear diatomic molecules (hydrogen and its isotopes, nitrogen, oxygen) do not have infrared absorptions. We have shown that the sensor response may be adequately predicted using commercially available software. Measurement of trace concentrations is limited by the broad spectral bandpass, since the total signal includes non-absorbed frequencies. However, cells with longer pathlengths can be designed to address this problem.

6.0 REFERENCES

-
- [1] Mauldin, C. B. , Gregory, C. M. *Proposal to Purchase Spare Finnigan MAT271 Mass Spectrometer and \$600,000 Spare Parts (U)*. TSD-APS-2001-00013, Savannah River Site, Aiken, SC 29808 (2001)
- [2] Mauldin, C. B., Levi, G. D. *Intermediate and Long Range Proposal to Maintain Analytical Capability for Tritium Processes (U)*. OBU-OLS-2004-00027, Savannah River Site, Aiken, SC 29808 (2004)
- [3] Powell, G. L. NSSE *GTIMOG ATAT Gas Sampling and Analysis*. YDZ-2436, Y-12 National Security Complex, Oak Ridge, TN (2003).
- [4] Marshall, Alan G., Hendrickson, Christopher L., Jackson, George S., *Mass Spectrometry Reveiws*, **1988**, 17, 1-35.
- [5] Veirs, K.; US DOE LBL-20565, UC-34A, **1985**.
- [6] Veirs, D. K. and Rosenblatt, G. M. *J Mol. Spectrosc.* **1987**, 121, 401-419.
- [7] Engelmann, U.; US DOE HNF-MR-0532, **1997**.
- [8] O'hira, S., Nakamura, H., Konishi, S., Hayashi, T., Okuno, K., Naruse, Y., Sherman, R. H., Taylor, D. J., King, M. A., Bartlit, J. R., and Anderson, J. L. *Fusion Tech* **1992**, 21, 465-470.
- [9] Sherman, R. H., Taylor, D. J., Bartlit, J. R., and Anderson, J. L., O'hira, S., Nakamura, H., Konishi, S., Okuno, K., and Naruse, Y. *Fusion Tech* **1992**, 21, 457-461.
- [10] Uda, T. O., K., and Naruse, Y. *Fusion Tech* **1992**, 21, 436-441.
- [11] Engelmann, U., Glugla, M., Penzhorn, R.-D., and Ache, H. J. *Fusion Tech* **1992**, 21, 430-435.
- [12] Myrick, M. L. and Angel, S. M. *Appl. Spectrosc.* **1990**, 44, 565-570.
- [13] Chong, C. K., Shen, C., Fong, Y., Zhu, J., Yan, F.-X., Brush, S., Mann, C. K., and Vickers, T. J. *Vib. Spectrosc.* **1992**, 3, 35-45.
- [14] Dao, N. Q. and Jouan, M. *Sens. Act. B* **1993**, 11, 147-160.
- [15] Berg, J. M., Rau, K. C., Veirs, D. K., Worl, L. A., McFarlan, J. T., Hill, D. D. *Appl. Spectrosc.* **2002**, 56, 83-90.
- [16] O'hira, S., Hayashi, T., Nakamura, H., Kobayashi, K., Yadokoro, T., Nakamura, N., Itoh, T., Yamanishi, T., Kawamura, Y., Iwai, Y., Arita, T., Maruyama, T., Kakuta, T., Konishi, S., Enoda, M., Yamda, M., Suzuki, T., Nishi, M., Nagashima, T., and Ohta, M. *Nucl Fus* **2000**, 40, 519.

-
- [17] Nave, S. E., O'Rourke, P. E., Malstrom, R. A., and Prather, W. S. *Proc. Control Qual.* **1992**, *3*, 43-48.
- [18] Nave, S. E.; US DOE WSRC-MS-96-0295, **1996**.
- [19] Malstrom, R. A.; US DOE SRT-ADS-97-0377, **1997**.
- [20] Moore, P. B., *System Design Description for HT-Thermal Cycling Absorption Process System and Hot and Cold Nitrogen Systems (U)*. X-SYD-H-00013 rev 8, **2003**.
- [21] Zeigler, K. E., Lascola, R. J., and Tovo, L. L., *Fiber Optic Laser Raman Spectroscopy Sensor (U)*. WSRC-TR-2003-000284, Rev.0.
- [22] Zeigler, K. E., *HT-TCAP Breakthrough Flow Tests Using an In-Line Fiber-Optic Raman Sensor (U)*. WSRC-TR-2004-00080, Rev. 0.
- [23] Poore, A., *HT-TCAP Material and Process Characterization Test Summary (U)*. WSRC-TR-2004-00275, Rev. 0.
- [24] Dickinson, T. A., White, J., Kauer, J.S., Wlat, D.R. *Nature* **1996**, *382*, 697-700.
- [25] Drew, S. M., Janzen, D.E., Buss, C.E., MacEwan, D.I., Dublin, K.M., Mann, K.R. *J. Am. Chem. Soc.* **2001**, *123*, 8414.
- [26] Drew, S. M., Janzen, D.E., Mann, K.R. *Anal. Chem.* **2002**, *74*, 2547-2555.
- [27] Drew, S. M., Mann, J.E., Marquardt, B.J., Mann, K.R. *Sens. and Act. B* **2004**, *97*, 307-312.
- [28] Rakow, N. A., Suslik, K.S., *Nature* **2000**, *406*, 710-713.
- [29] Daws, C. A., Exstrom, C.L., Sowa, J.R., Mann, K.R. *Chem. Mater.* **1997**, *9*, 363-368.
- [30] Exstrom, C. L., Sowa, J.R., Daws, C.A., Janzen, D., Moore, G.A., Stewart, F.F., Mann, K.R. *Chem. mater.* **1995**, *7*, 15-17.
- [31] R.S. Willms and K. Okuno, "Recovery of hydrogen from impurities using a palladium membrane reactor", Proc. 15th IEEE Symp. On Fusion Eng., Hyannis, MA, Oct. 11-15, 1993, 85-90.
- [32] S.A. Birdsell, R.S. Willms, P. Arzu, and A. Costello, "Effect of inlet conditions on the performance of a palladium membrane reactor", Proc. 17th IEEE/NPS Symp. on Fusion Eng., San Diego, CA, Oct 6-10, 1997, 301-303.
- [33] S.A. Birdsell and R.S. Willms, "Tritium recovery from tritiated water with a two-stage palladium membrane reactor", *Fusion Eng. and Design* **39-40** (1998) 1041-1048.
- [34] K.D. Cleaver, "The analysis of process gases: a review", *Accred. Qual. Assur.* **6** (2001) 8-15.

-
- [35] P.T. Jaakkola *et al.*, “On-line analysis of stack gas composition by a low resolution FT-IR gas analyzer”, *Water, Air, and Soil Pollution* **101** (1998) 79-92.
- [36] J. Bak and S. Clausen, “FTIR emission spectroscopy methods and procedures for real time quantitative gas analysis in industrial environments”, *Meas. Sci. Technol.* **13** (2002) 150-156.
- [37] I. Linnerud, P. Laspersen, and T. Jaeger, “Gas monitoring in the process industry using diode laser spectroscopy”, *Appl. Phys. B* **67** (1998) 297-305.
- [38] G. Berden, R. Peeters, and G. Meijer, “Cavity ring-down spectroscopy: Experimental schemes and applications”, *Int. Rev. Phys. Chem.* **19** (2000) 565-607.
- [39] P.A. Wilks, “In-line infrared sensors covering the mid-infrared from 2 to 14 μ m (5000 to 700 cm^{-1})”, *Proc. SPIE* **4577** (2002) 76-82.
- [40] W. McKinney, Black Body Emission Calculator, <http://infrared.als.lbl.gov/calculators/bb2001.html>, 2001.
- [41] David R. Lide, ed., *CRC Handbook of Chemistry and Physics, Internet Version 2005*, <<http://www.hbcpnetbase.com>>, CRC Press, Boca Raton, FL, 2005.
- [42] L.S. Rothman *et al.*, “The HITRAN molecular spectroscopic database: edition of 2000 including updates through 2001”, *J. Quant. Spectrosc. Rad. Transfer* **82** (2003) 5-44.
- [43] W. Demtröder, *Laser Spectroscopy*, 3rd printing, Springer-Verlag, Berlin, 1988.

ACKNOWLEDGEMENTS

The authors thank Tritium Facility start up personnel and process engineers, especially Kevin Sessions, Janine Horn, Danny Epting, and Blake Moore, for their help and support in demonstrating the fiber optic Raman sensor during cold runs.

We would like to thank H. T. Sessions of SRNL for assistance with incorporation of the miniature infrared sensor into the PMR manifold.